

Fall 12-2015

Experimental and Computational Investigation of Ribbed Channels for Gas Turbine Thermal Management

Yash T. Mehta
Embry-Riddle Aeronautical University

Follow this and additional works at: <https://commons.erau.edu/edt>



Part of the [Aerospace Engineering Commons](#)

Scholarly Commons Citation

Mehta, Yash T., "Experimental and Computational Investigation of Ribbed Channels for Gas Turbine Thermal Management" (2015). *Doctoral Dissertations and Master's Theses*. 227.
<https://commons.erau.edu/edt/227>

This Thesis - Open Access is brought to you for free and open access by Scholarly Commons. It has been accepted for inclusion in Doctoral Dissertations and Master's Theses by an authorized administrator of Scholarly Commons. For more information, please contact commons@erau.edu.

EXPERIMENTAL AND COMPUTATIONAL INVESTIGATION OF RIBBED
CHANNELS FOR GAS TURBINE THERMAL MANAGEMENT

A Thesis
Submitted to the Faculty of
Embry-Riddle Aeronautical University

by

Yash T. Mehta

In Partial Fulfillment of the
Requirements for the Degree of
Master of Science in Aerospace Engineering

December 2015
Embry-Riddle Aeronautical University
Daytona Beach, Florida

EXPERIMENTAL AND COMPUTATIONAL INVESTIGATION OF RIBBED
CHANNELS FOR GAS TURBINE THERMAL MANAGEMENT

by

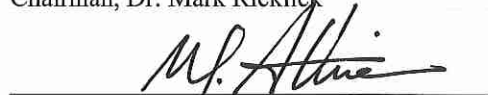
Yash T. Mehta

A Thesis prepared under the direction of the candidate's committee chairman, Dr. Mark Ricklick, Professor, Department of Aerospace Engineering, and thesis committee members Dr. Magdy Attia, Professor, and Dr. Sathya Gangadharan, Professor, and has been approved by the members of the thesis committee. It was submitted to the School of Graduate Studies and Research and was accepted in partial fulfillment of the requirements for the degree of Master of Science in Aerospace Engineering.

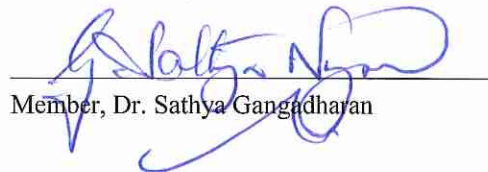
THESIS COMMITTEE



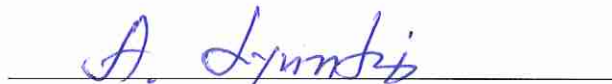
Chairman, Dr. Mark Ricklick



Member, Dr. Magdy Attia

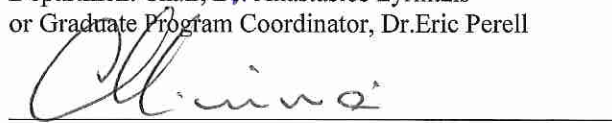


Member, Dr. Sathya Gangadharan



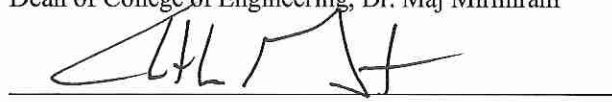
Department Chair, Dr. Anastasios Lyrantzis
or Graduate Program Coordinator, Dr. Eric Perell

12/2/15
Date



Dean of College of Engineering, Dr. Maj Mirmirani

12/2/15
Date



Associate VP for Academics, Dr. Christopher Grant

12/4/15
Date

ACKNOWLEDGMENTS

First and foremost I would like to express my appreciation to my thesis advisor Dr. Mark Ricklick for all the support, guidance and information provided which facilitated my master's thesis. Without his motivation and stride to have everything perfect, the completion of this project wouldn't have been possible. Thank you for letting me be a part of the Propulsion Thermal Management Laboratory (PTML) research team.

Furthermore I would like to extend my gratitude to my thesis committee members; Dr. Magdy Attia and Dr. Sathya Gangadharan whose instructions and comments helped me get better in the avenues of gas turbine engines. Taking classes with them was truly an honor, which helped me develop my interests in the applications of fluid flow and turbine engine propulsion. All these 3 professors trained me to think outside the box and prepared me for the industry ahead.

Finally I would also like to acknowledge my lab mates, Bhushan Upalkar and Royce Fernandes who played a vital role in starting and setting up the experimental facility for the PTML at Embry-Riddle. I would like to dedicate this work to my academic peers, friends and most importantly my family whose constant support and motivation helped me push my limits and achieve my goals. Without the continued support of my dad, my mom's tears and sister's motivation, this wouldn't have been possible.

TABLE OF CONTENTS

LIST OF TABLES	v
LIST OF FIGURES	vi
SYMBOLS.....	viii
ABBREVIATIONS	ix
ABSTRACT.....	x
1. Introduction	1
1.1. Motivation.....	1
1.2. Thermodynamics	2
1.3. Turbine Blade Cooling.....	5
1.3.1. Rib-Turbulated Channel Cooling	6
2. Literature Review	10
2.1. Turbine blade cooling.....	10
2.2. Rib Turbulated cooling.	10
3. Methodology and Set-Up	19
3.1. Introduction.....	19
3.2. Computational Setup.....	20
3.2.1. Computational Domain and Model Set-Up	20
3.2.2. Meshing and Turbulence.....	23
3.3. Experimental Setup	28
3.3.1. General Rig Description.....	28
3.3.2. Ribbed Channel Setup.....	34
3.4. Data Reduction	35
4. Results and Analysis	38
4.1. Smooth Channel Validation (Experimental)	38
4.2. Ribbed Channel Benchmarking (CFD).....	39
4.2.1. Benchmarking to JC Han	39
4.2.1.1. Pressure Data and Friction Factor	40
4.2.1.2. Heat Transfer Analysis.....	42
4.3. PTML Ribbed Channel Data	47
4.3.1. CFD Analysis	47
4.3.2. Experimental Analysis	49
5. Conclusion.....	53
6. Recommendations	55
7. Publications Resulting from this work	56
REFERENCES	57
A. Appendix	60

LIST OF TABLES

Table 4-1: Friction factor comparison to Han's (1985) data (Percent Diff.)	42
Table 4-2: Local Nusselt number comparison between experimental & CFD models ...	46

LIST OF FIGURES

Figure 1-1: Ideal Brayton Cycle	2
Figure 1-2: Turbine inlet temperatures over the years (Clifford, 1985)	3
Figure 1-3: Stages of a Gas turbine engine (Wikipedia).....	4
Figure 1-4: Various cooling techniques (JC Han, 2010)	6
Figure 1-5: Flow separation and reattachment around ribs (Han, 1985).	8
Figure 2-1: Nusselt number correlations for different wall in the channel (Kiml, 2001). 12	
Figure 2-2: Various Rib Configurations used to Enhance Internal Heat Transfer (Han, 2006)	13
Figure 2-3: Flow structure for different rib pitch-to-rib height ratios (Han, 1978).	16
Figure 2-4: Different types of perforated ribs (Buchlin, 2002).	16
Figure 2-5: The heat transfer coefficients after the perforated rib (Buchlin, 2002).	17
Figure 3-1: Flowchart of the goals of this project.....	19
Figure 3-2: Various geometric parameters of the channel (Han, 1985).	20
Figure 3-3: Representation of the channel setup.....	21
Figure 3-4: Section modelled in CFD	22
Figure 3-5: The Domain Set-up	23
Figure 3-6: Mesh sizes and cell quality around the rib.	24
Figure 3-7: Avg. surface temperature and avg. Nusselt number vs. Cell count (Basesize)	25
Figure 3-8: Y+ contour for the side wall.	26
Figure 3-9: Y+ contour for the bottom ribbed wall.	26
Figure 3-10: CAD model for the experimental rig test section	29
Figure 3-11: Experimental blower used with control valves.	30
Figure 3-12: Flow loop of the experimental rig.....	30
Figure 3-13: Arrangement of the heater strips on the bottom wall	31
Figure 3-14: Test rig set up along with LED, Camera, and Traverse in the dark room ...	33
Figure 3-15: Test section bottom wall painted with Temperature Sensitive Paint.	34
Figure 3-16: Ribbed channel test rig setup - Bottom wall	35
Figure 3-17: Ribbed channel test rig setup - Top wall.....	35
Figure 4-1: Velocity profiles at the boundary layer (Chklovski).....	38
Figure 4-2: Experimental vs. CFD Velocity profiles.....	39
Figure 4-3: Residuals for time averaged iterations.	40

Figure 4-4: Friction factor for varied α experimentally compared to CFD at $P/e = 10$	41
Figure 4-5: Nusselt Number contours for EBKe and V2F models on the side wall.....	43
Figure 4-6: Nusselt Number contours for EBKe and V2F models on the bottom wall....	43
Figure 4-7: Span averaged Nusselt number variation on the Ribs.....	44
Figure 4-8: Fully developed region for Nusselt number variation (Zoomed In)	45
Figure 4-9: J.C. Han's Local Nusselt number values for $\alpha = 90^\circ$	46
Figure 4-10: Velocity and Wall Shear Stress contours showing the reattachment lengths for EBke and V ² F.....	47
Figure 4-11: Computational span averaged Nusselt Number along the bottom wall.	48
Figure 4-12: Nusselt number contour for EBk- ϵ model at Re of 21,500.....	49
Figure 4-13: Experimental Contour for Temperature.....	50
Figure 4-14: Experimental Contour for Nusselt Number	50
Figure 4-15: Experimental span averaged Nusselt Number along the bottom wall at Re = 21,500.....	51
Figure 4-16: Experimental span averaged Nusselt Number along the bottom wall at Re = 42,000.....	52
Figure 6-1: Images for different geometries tried in OPTIMATE+	55

SYMBOLS

ε	Turbulent Dissipation Rate (Tdr) or Strain Energy
η	Efficiency
ϖ	Strain Energy per unit volume
D	Hydraulic Diameter
f	Friction Factor
H	Heat transfer coefficient
I	Intensity of the paint
I_r	Reference Image Intensity of the paint
k_{air}	Thermal Conductivity of Air
k_I	Thermal Conductivity of Inconel
K	Turbulent kinetic energy (Tke)
M	Mach Number
\dot{M}	Mass flow rate
Nu	Nusselt Number
Pr	Prandtl Number
P_s	Static Pressure
P_0	Total Pressure
Re	Reynolds Number
Sc	Schmidt Number
T	Temperature
T_3	Turbine Inlet Temperature
T_4	Turbine Exhaust Temperature
T_w	Temperature of the wall
Tr	Reference Temperature of the fluid
x	Distance in Stream wise direction
X/D	Stream wise distance in terms of hydraulic diameter

ABBREVIATIONS

CFD	Computational Fluid Dynamics
CAD	Computer Aided Design
RANS	Reynolds Averaged Navier Stokes
LES	Large Eddy Simulation
DNS	Direct Numerical Solution
BR	Blowing Ratio
EB	Elliptic Blending
STAR-CCM+	Simulation of Turbulence in Arbitrary Regions-Computational Continuum Modeling
CCD	Charge Coupled Device
TSP	Temperature Sensitive Paint
PSP	Pressure Sensitive Paint
LED	Light Emitting Diodes
DB	Dittus-Boelter

ABSTRACT

Researcher: Yash T. Mehta

Title: Experimental and Computational Investigation of Ribbed Channels for Gas Turbine Thermal Management.

Institution: Embry-Riddle Aeronautical University

Degree: Master of Science in Aerospace Engineering

Year: 2015

This study focuses on the computational benchmarking as well as validation against experimental results of a rib roughed surface in an internal channel of a stationary turbine blade. STAR-CCM+ was utilized to replicate a model from a published article, and to analyze the CFD conjugate heat transfer by determining the turbulence model that best matched the published experimental values. Using those computational conditions and CFD results, an in house experimental rig was validated by comparing convective heat transfer coefficients and pressure profiles. This cooling method, when compared to a smooth channel, enhances turbulent mixing by separating and reattaching the boundary layer which increases the heat transfer. The overall goal is to analyze an effective cooling method, studying the flow physics and effective heat transfer rates as well as minimizing the pressure drop across the channel. V^2f turbulence model resulted in matching closest to the experimental results, but due to its unstable nature at high Reynolds number, the EBk- ϵ model was used for preliminary testing. Results for EBk- ϵ showed shorter reattachment lengths giving higher Nusselt number values between the ribs. The heat transfer as well as friction factors match within the uncertainty of 6.8% and 6.6% respectively of the published results. Benchmarked computational results will help validate the experimental setup for further optimization and testing different configurations in rib arrangements.

1. Introduction

1.1.Motivation

The constant need for power and energy gives more scope for the production of it. Different modes of power generation are widely used today including land based, water based, air based etc. One of the most extensively used machine to generate large amounts of power is the gas turbine engine, which is used to power almost all aircraft used today as well as land based power plants. Thermal energy is converted into work (thrust) which helps propel such large masses into the air. Gas turbine engines are governed by the principles of the Brayton cycle which includes compression of air, adding heat and converting that heat into work which in turn provides power for the aircraft.

Constant advancements in aircraft engines have done nothing but increase its efficiencies, build better aerodynamically advanced parts, lesser overall weight, long distance travels etc. But in effect of all this, a lot of other factors are involved one of which is the turbine cooling techniques used. The turbine is connected to the compressor via a shaft which propels it by the force of the air coming out of the combustion chamber. These adiabatic flame temperatures are of the of magnitudes of 1500 - 2000° C which is higher than the melting points of most of the materials used to cast engine blades and components. Hence in order to maximize the use of turbine blades without being changed constantly, internal cooling is very necessary because increasing the turbine inlet temperature helps increase the efficiency of the gas turbine. Limitations to internal cooling come into play due to the complexity of different cooling techniques and the rate at which it needs to be cooled.

1.2. Thermodynamics

The performance of a gas turbine is governed by an isentropic process of the Brayton Cycle which follows an open cycle process. Figure 1-1 below shows a basic Brayton cycle

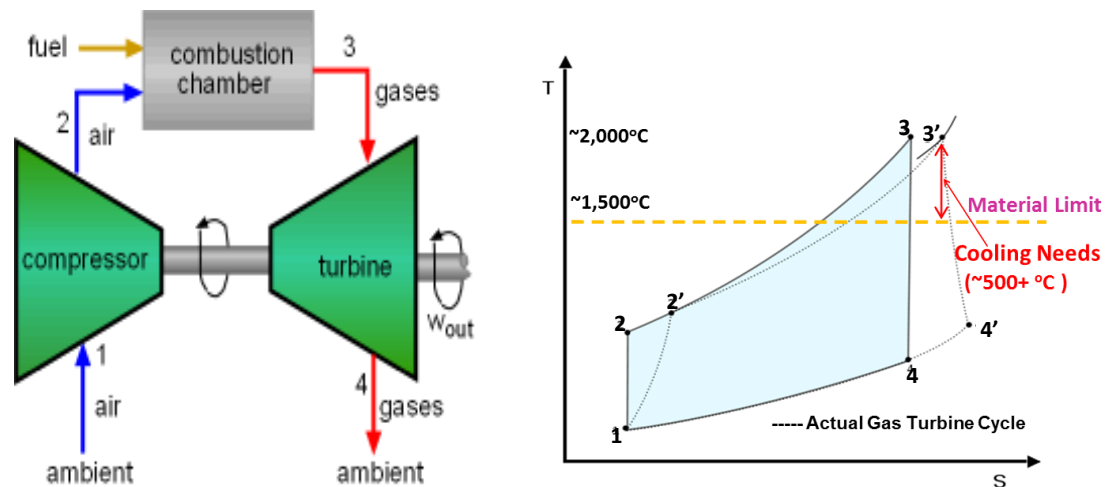


Figure 1-1: Ideal Brayton Cycle

As seen in the Brayton cycle, the ambient air enters the compressor where the air is compressed and the air pressure is raised considerably. This compressed air is then mixed with fuel in the combustion chamber and ignited which adds heat. This air then turns the turbine which is connected to the compressor, and hence turns the compressor as well. The adiabatic flame temperatures exiting the combustion chamber range around 1500 – 2000°C using the standard fuels used today. Most materials used to make the turbine blades and the casing around it, cannot withstand such high temperatures. The super alloys used, fail at temperatures of 1100°C or less. Due to the limitations with component materials, the T3 which is the turbine inlet temperature is considerably lowered which reduces the overall efficiency.

The Brayton cycle efficiency is given by:

$$\eta = 1 - \frac{(T_4 - T_1)}{(T_3 - T_2)} \quad (1)$$

With the governing Brayton cycle, there are various performance benefits but over the years it has also seen some inefficiencies. Mechanical losses, compressor losses as well as expander losses are some of the few which directly impact the overall work outputted from the system. As we know that increasing the compression ratio of the cycle boosts the efficiency of the system and that would be the most affected solution to such a problem. But in doing so, the temperature of the overall core flow entering the turbine is drastically increased which boils down to the same problem of component failure. Figure 1-2 below shows the increase in turbine inlet temperatures over the years due to the advancements in cooling techniques to mitigate the metallurgical failure.

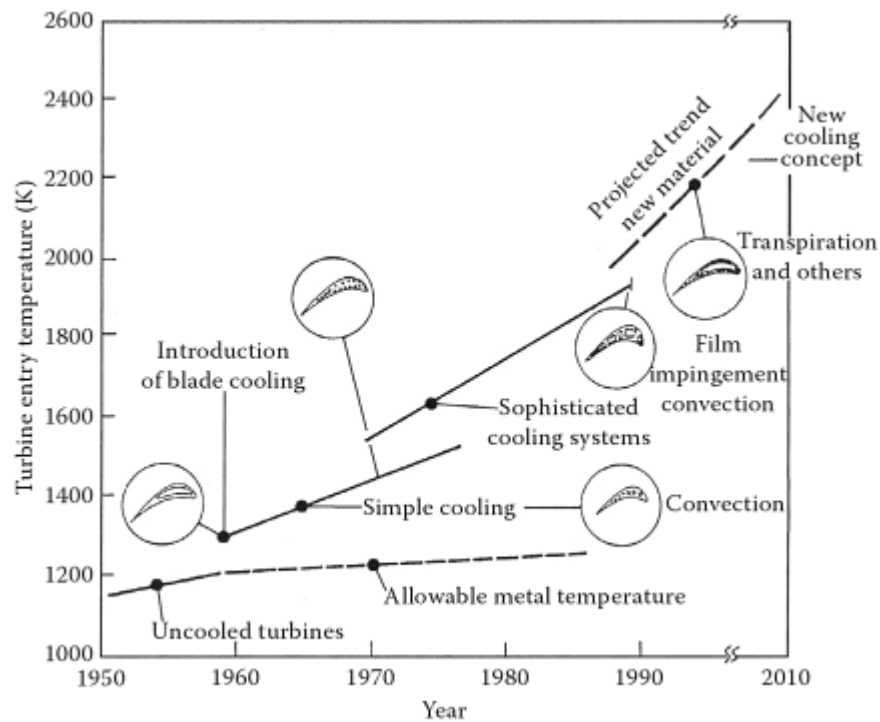


Figure 1-2: Turbine inlet temperatures over the years (Clifford, 1985)

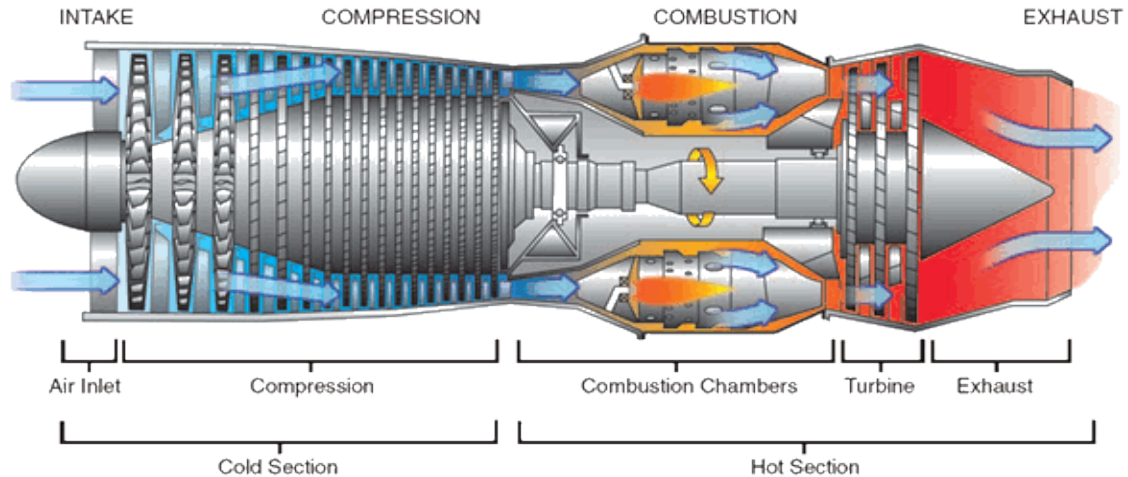


Figure 1-3: Stages of a Gas turbine engine (Wikipedia).

As seen in Fig. 1-3, mainly the first stage of the turbine experiences very high heat loading as it is directly situated after the combustion chamber, thus having high internal heat transfer rates is a must. Achieving those heat interactions requires high concentrations of cooling air inside the internal channels most of which comes from the bleed air from the compressor. The air which is bled from the compressor stands at about 650°C , which when interacts with the hot gases, lowers the blade temperature to about 1000°C , which is permissible for reliable operation of the engine. It is evident that the efficiency of the system is hampered if large amounts of air is bled. Thus in order to enhance the cooling effect, the right proportion of bleed air is required to minimize metal failure. It is of natural occurrence that as the turbine inlet temperature increases, the amount of heat generated is increased which is converted into thrust. This is very well highlighted by the fact that a 56 Kelvin increase in hot gas temperature potentially yields an increase of up to 13% in power output or 4% in simple cycle efficiency (Hyung Hee, 2011). Due to these high temperatures, a lot of thermal stresses and thermal loading is witnessed on the turbine blades. Hence turbine cooling has become one of the vital aspects to increase the overall life of the aircraft engine.

1.3. Turbine Blade Cooling

To counter the ever rising demands of smaller, light weight and efficient gas turbine engines, increasing the turbine inlet temperatures is one of the easiest options. Hence catching up to those demands give rise to innovations in the turbine cooling sector. Hence come the need of effective and accurate cooling techniques. Life of a turbine blade can be reduced by half if the temperature predictions of the metal blade are off by only 30°C. In order to avoid premature failures or disasters, the designers need to accurately predict the local heat transfer coefficients and local airfoil metal temperatures. Another way to increase life of the blades would be mitigating local hot spots which is also a major reason for material failures. Over the past decades, turbine blades have not only progressed in adhering to high temperatures but also bear high stress loading and drastically changing environmental conditions which has helped boost the life limit of the overall machine. Figure 1-4 shows the various cooling techniques used to safely operate a turbine blade at high temperatures.

As seen there are 2 main types of cooling, external and internal cooling. External cooling include showerhead and film cooling which save the blade from the hot gas being driven through the passage. This is done by retaining a layer of relatively cooler air, protecting them from the hot gases. On the flip side, internal channel cooling has various different options to offer. With the common impingement cooling holes situated in the leading edge areas of the blade, it impinges cool air from the channel closest to the outer region of the blade causing it to enhance heat transfer. The trailing edge is dominated by pin fins which are typically cylinders used to increase structural support and providing a great tool for heat transfer between the outer and inner regions of the blade. The mid

chord region of the internal channel most commonly sees ribs or dimples to enhance heat transfer. Analyzing the flow over a rib is the main interest of this study. However, due to complex flows around the airfoils as well as within the internal channels, it has been difficult for designers to accurately predict metal temperatures.

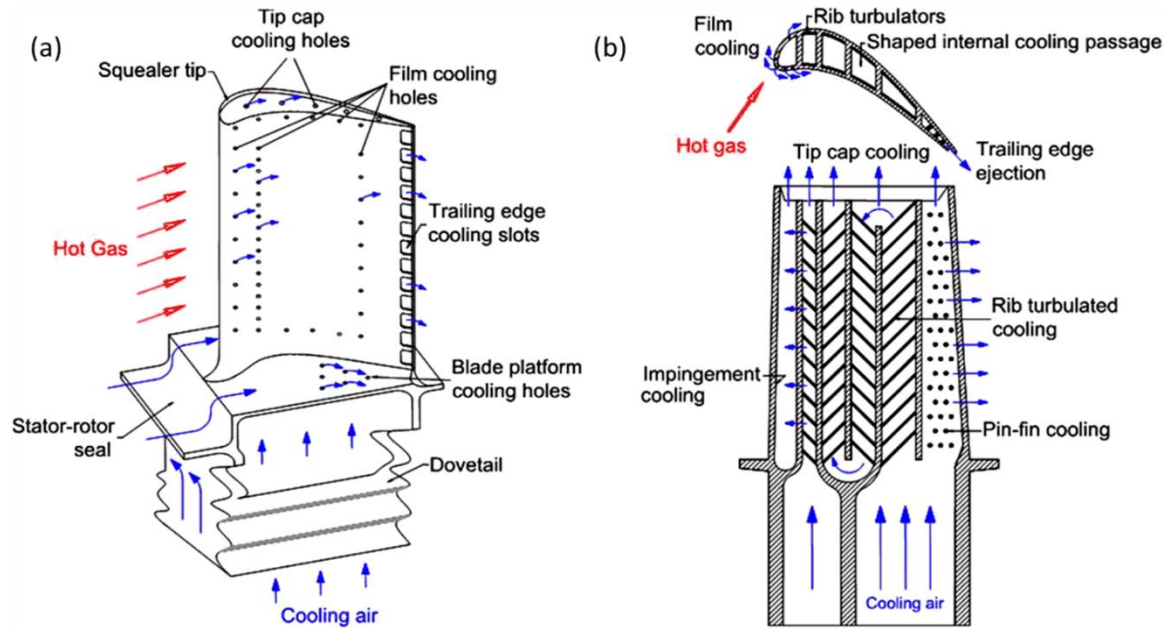


Figure 1-4: Various cooling techniques (JC Han, 2010)

1.3.1. Rib-Turbulated Channel Cooling

Ribs are protrusions which are placed in a controlled way along specific target walls of the internal duct. Repeated rib turbulence promoters are cast on the two opposite walls (pressure and suction sides) of the internal duct to enhance the heat transfer. Having ribs on the opposite walls, maximizes the interaction with the coolant and wall and helps cool the turbine blade effectively. Various cases see ribs only on one side of the duct because they need to match the external thermal loads which are different for the pressure and suction sides. While it causes friction for the flow in the channel which is correlated

to increased heat transfer, its drawback is pressure drop, which will be higher than a regular smooth channel. Hence having the right rib-height, rib pitch and the angle at which the ribs hit the flow is very important to minimize pressure loss and maximize benefits.

Ribs have conventionally been arranged orthogonally to the flow, i.e., the extension of the rib is situated 90° to the streamwise flow direction. Different configurations for the rib placement like the angle of attacks have different characteristics and hence different heat transfer rates. As per previous studies, the rib pitch-to-height ratio (P/e), the rib height-to-hydraulic diameter (e/D) and rib angle of attack are the main factors effecting the heat transfer coefficients and friction factors (Han, 1985).

The function of a rib is to detach a layer of the oncoming flow as the rib is placed in such a way that it obstructs a part of the flow. Due to the presence of the rib, the flow trips and separates at the top of the rib and reattaches to the wall between the ribs. The boundary layer is disturbed increasing the turbulence of the flow due to the separation and reattachment. Due to this phenomenon, the flow mixes the fluid elements near the wall with the cooler air in the middle of the flow, enhancing the overall heat transfer. The fact that it only disturbs the near – wall flow, the overall heat transfer of the flow is enhanced and the pressure drops are relatively low (Zuckerman, 2005). This can be clearly visualized in Fig. 1-5 which shows how the flow is separated and reattached between two ribs.

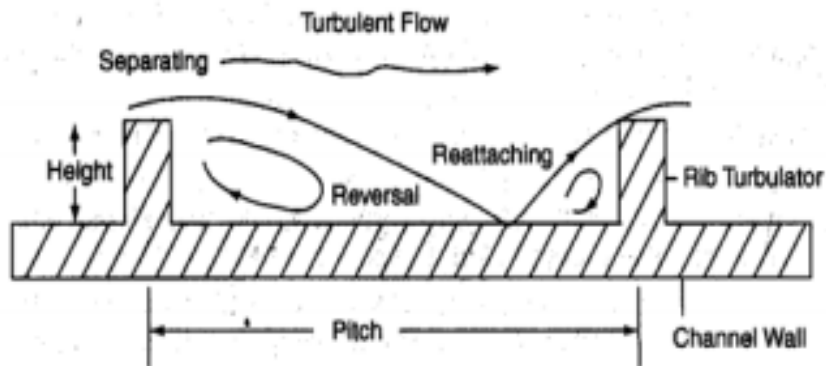


Figure 1-5: Flow separation and reattachment around ribs (Han, 1985).

The flow around a rib is characterized by several re-circulating zones which involves shear, mixing, and impinging flow which increases the turbulence level and hence the heat transfer to 2-4 times that experienced in a smooth channel. The main effect is the large re-circulating zone downstream of the rib and the reattachment length. The physics within this region is similar to that behind a backward-facing-step.

The ribs are represented as short, rectangular or square channels with different aspect ratios (AR). In case of a rectangular channel, the enhancement of heat transfer is dependent on the rib turbulators' geometry, such as rib size, shape, distribution, flow angle of attack, and the flow Reynolds number. To obtain higher Reynolds number (Re) flows, the rib height should be constrained in order to receive higher efficiencies with a hit on the heat transfer coefficient and increased pressure drop (Florschuetz, 1981). Rib spacing is widely effective on the performance of the channel as closely spacing the ribs would enhance the heat transfer but spacing them wider would increase the overall area for convection. Hence optimization of the rib is a key aspect in order to obtain optimal results for heat transfer.

In order to assess the performance of the rib in a smooth channel, different comparison factors are studied to evaluate the best results. In most cases Nusselt number (Nu) and friction factor (f) are analyzed because small changes in the rib geometry can be easily tracked. In case of the rib, thermal energy is transferred from the external pressure and suction surfaces of the turbine blades to the inner zones through conduction which is then removed by internal cooling.

2. Literature Review

2.1. Turbine blade cooling

Internal channels of a turbine blade are mostly modeled as short, square or rectangular channels with various aspect ratios. Keeping in mind the serpentine path it sees inside the turbine blade, the heat transfer augmentation primarily depends on the geometry of the mixing within the duct, the flow attach angle and the flow Reynolds number.

Continuous gas turbine cooling methods and concepts have allowed the turbine inlet temperatures to increase over the years. Even with the advancements in super alloys, the metallurgical limits to withstand the hot gasses haven't reached the maximum possible temperatures. Thus component cooling is required in order to play the balance between increasing turbine inlet temperatures as well as boost the overall system efficiency. As stated by Boyce (2006), advancements in materials have only given an increase of 4°C in turbine firing temperatures per year. Whereas advance cooling techniques contributed to 11°C increase of turbine inlet temperature per year.

2.2. Rib Turbulated cooling.

Turbulence promoters are introduced in the internal cooling passage for heat transfer enhancements. The most common turbulence promoters are so-called the rib-turbulators, that typically oriented at certain angle transverse to the flow direction and formed as an integral structural part of the airfoil inner wall. There has been numerous studies that have been conducted over the years on a wide range of rib configurations in various size cooling channels using many experimental techniques. Rib-turbulators are

often cast on both walls of the internal cooling passages that have two-dimensional structures and are mainly used in the serpentine passages to cool the mid-chord region of an airfoil. There are vast literatures available about rib-turbulated cooling conducted in non-rotating channels that involve different amalgamations of rib height, rib angle, rib spacing, rib shape, and inline or staggered rib configurations.

Typically, the rib height to hydraulic diameter (e/D) ranges by about 5-10% of the entire cooling passage, the rib spacing-to-height ratio also known as the Pitch-to-height ratio (P/e) varying from 5 to 20, and a rib flow attack angle around 30° - 60° in addition to the 90° flow which is perpendicular to the mainstream flow (Han, 2006). For higher Reynolds number flows, it is stated that smaller ribs are more efficient but due to the high speeds, the heat transfer enhancements decrease. Also for higher Reynolds number flows, the friction factors increase which causes an increased penalty in pressure drop.

J.C Han (1988) investigated orthogonal ribs as well as angled ribs and determined that placing ribs at an angle to the main flow of the channel compared to the 90° ribs would give a higher rate of heat transfer. This is also backed by various other studies by Han and Park (1988) and Park et al. (1992) where they investigated the thermal performance of angled ribs compared to orthogonal ribs.

Kim, Mochizuki and Murata, (2001) analyzed the effects of rib arrangements on heat transfer and flow behavior in a rectangular rib-roughed passage. In the study they modeled a 2:1 aspect ratio rectangular channel with four configurations of angled ribs (90° , 75° , 60° and 45°). They claimed that in order to enhance the heat transfer of the bottom wall, the oblique ribs should be arranged so that the secondary flow along the ribs hits the top wall instead of the bottom wall because it turns back and carries the cold air

from the core passage region to the bottom wall. Hence they concluded that the 60° rib pattern achieved the maximum heat transfer due to strong rotational momentum of the secondary flow. Fig. 2-1 below shows the heat transfer rates for different rib orientation on all four walls.

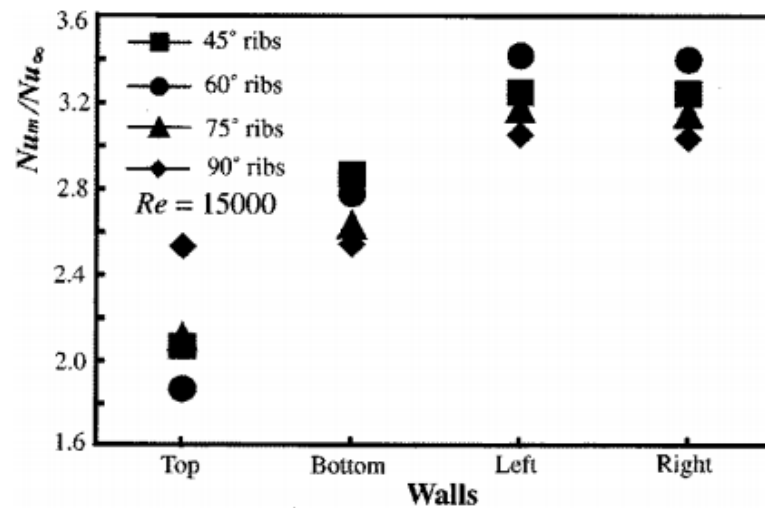


Figure 2-1: Nusselt number correlations for different wall in the channel (Kiml, 2001)

Han et al. (2000) mentioned that in some highly demanding cooling designs, larger rib height-to-channel hydraulic diameter ratio can be used to generate higher heat transfer enhancement provided pressure penalty is not a main concern.

Fig. 2-2 below shows several rib configurations that have been studied by different groups of researchers (Han, 2006).

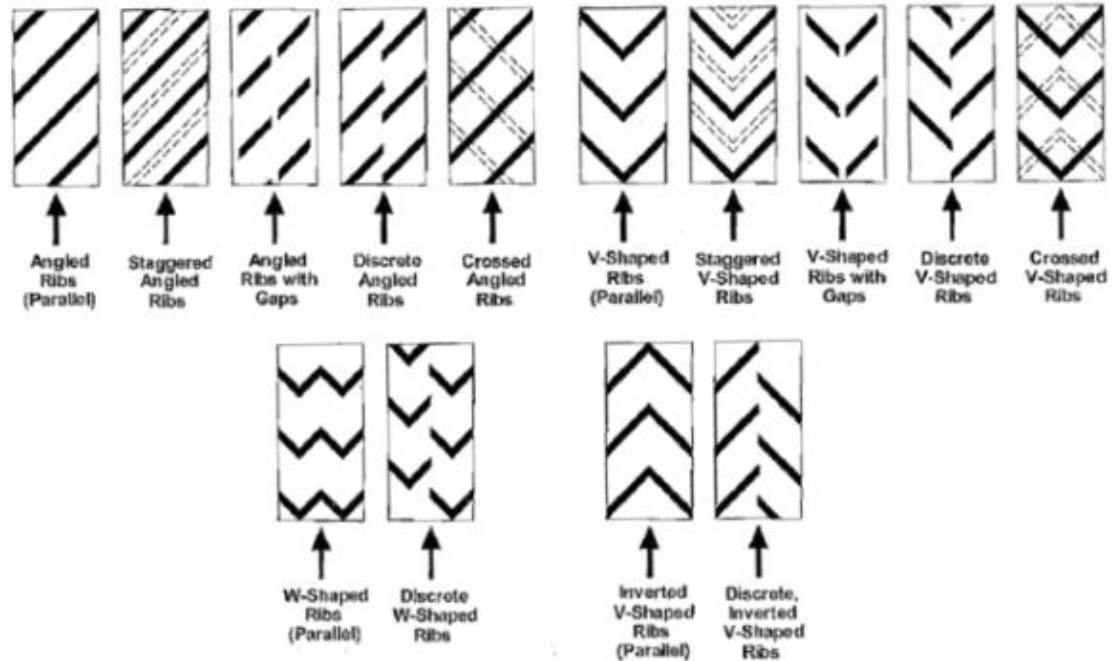


Figure 2-2: Various Rib Configurations used to Enhance Internal Heat Transfer (Han, 2006)

Rau et al. (1998) measured the local heat transfer performance in a ribbed roughened square channel with blockage ratio (rib height-to-hydraulic diameter of the channel – e/D) of 10 to 20%. They found that the strong secondary flows results in a three-dimensional flow field with high gradients in the local heat transfer distributions on the smooth side walls. They concluded that the correlation used for predicting heat transfer in a ribbed channel with smaller e/D ratio does not work for a higher e/D ratio channel.

Ekkad and Han (1997) studied heat transfer distributions in two-pass square channels with rib turbulators using a transient liquid crystal technique. Four configurations of 90° parallel, 60° parallel, 60° V-shaped, and 60° inverted V-shaped ribs were discussed. They noted that the periodic ribs break the laminar sublayer and create

local wall turbulence due to flow separation and reattachment between the ribs, greatly enhancing the heat transfer (Ekkad, 1997). They also found that Nusselt number ratios are highest on top of the ribs and lowest immediately before and after the ribs for all ribbed channels.

Han, et al. (1991) studied the effect of the rib angle orientation on local heat transfer distributions and pressure drop in a non-rotating square channel with opposite, in-line ribbed walls. They found that the 60° and 45° V-shaped ribs performed better than the 60° and 45° crossed ribs or 90° transverse ribs. “The V-shaped rib produces the highest heat transfer augmentation while the inverted V-shaped rib generates the greatest pressure drop” (Han et al., 1991).

The focus of rib turbulators began to shift to the investigation of “high performance” ribs. Han et al. (1991) studied a square channel with V, Λ , parallel (angled), and crossed ribs. They showed the V-shaped ribs (45° and 60°) perform better than the parallel ribs (45° and 60°).

Wang et al. (2001) performed experiments to study the local heat transfer and pressure drop characteristics of developing turbulent flows of air in three different types of ribbed ducts. These include the constant cross section square duct, the diverging square duct and the converging square duct. When analyzing the 3 ducts, it was seen that the diverging duct showed the highest heat transfer characteristics while constant cross section duct was found better than the converging duct.

Another study for heat transfer and friction losses in a square channel with 90° ribs on one, two, three and four walls was conducted by Chandra et al. (2003). They performed the experiments with the Reynolds numbers varying from 10,000 till 80,000. It

was found that with increase in ribbed walls the thermal performance decreases due to increase in pressure drop.

The Pitch that is the distance between the trailing edge of one rib to the trailing edge of the second consecutive rib plays a vital role in creating turbulence. It effects the separation and reattachment of the flow, thus it affects the heat transfer enhancement in the channel. Han et al. (1978), has experimentally showed that the maximum heat transfer is obtained for Pitch-to-rib height ratio (P/e) of 10. Below this value the reattachment between the ribs was not visible. Figure 2-3, shows the separation and reattachment of flow phenomenon for different P/e ratios. For a P/e of less than 7, there exist a separation bubble on top of each rib. When P/e is equal to 7, the boundary layer between the separation zones and on the ribs does not develop. For P/e equal to 10, which is believed to be the optimal value as maximum heat transfer is achieved, the re-attachment occurs between the ribs while the separation bubble at top of the ribs extend past the back of the rib and combine with the separation region following the rib. Thus at $P/e = 10$, maximum break-up of near wall flow is achieved which results in increase in turbulence level and enhance the exchange of fluid in the near wall region with the core flow.

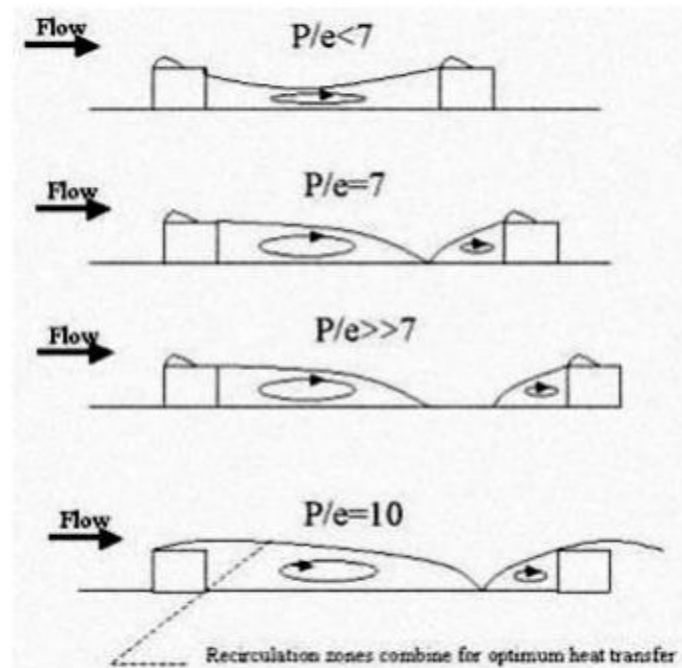


Figure 2-3: Flow structure for different rib pitch-to-rib height ratios (Han, 1978).

Buchlin, (2002) studied the convective heat transfer in a channel with perforated ribs. She modeled different types of perforations in a single rib turbulator in order to predict the highest heat transfer. Infrared thermography with a steady heated thin foil technique was used to obtain the mapping of heat transfer coefficients. The Chevron type of perforation was studied in detail. It was concluded that increasing the open-area ratio of the perforated rib up to 36% and Reynold's number higher than 20,000 improves the heat transfer significantly.

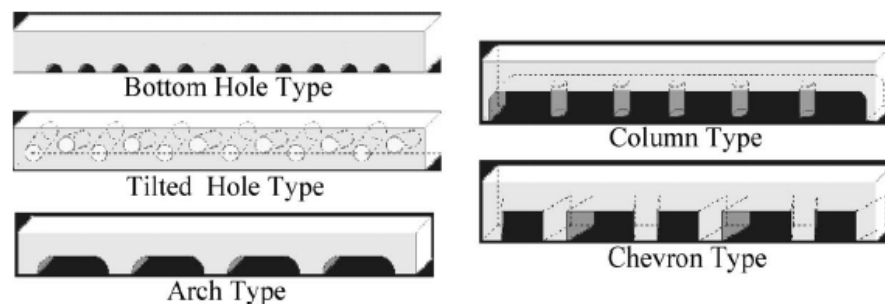


Figure 2-4: Different types of perforated ribs (Buchlin, 2002).

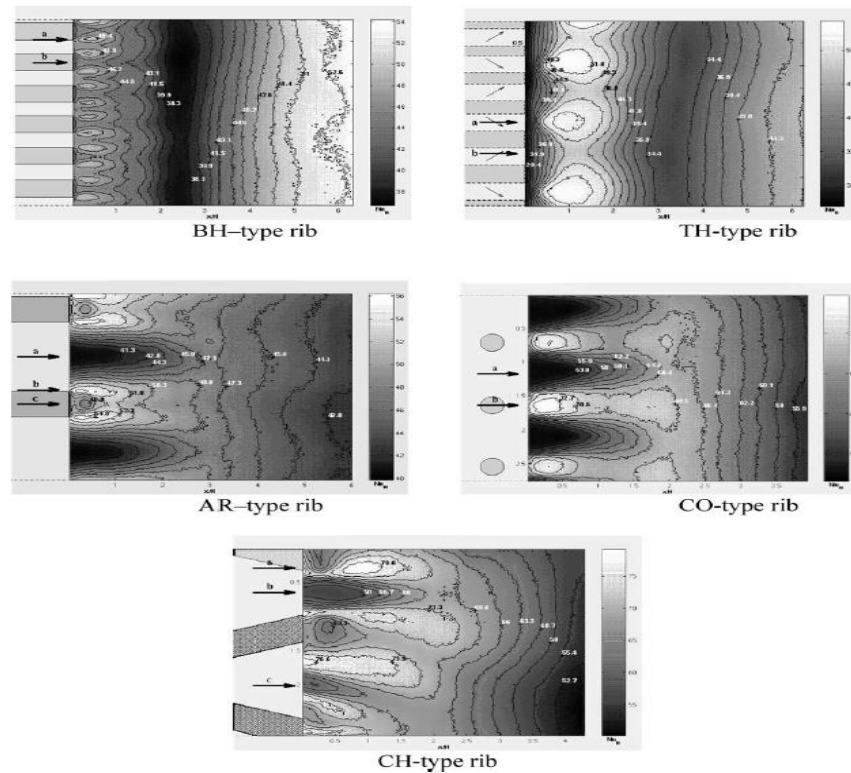


Fig. 6. Mapping of the heat transfer coefficient: $Re_H = 22000$.

Figure 2-5: The heat transfer coefficients after the perforated rib (Buchlin, 2002).

Kim, Rhee et al. (2004) investigated the duct aspect ratio effects on the mass transfer in a rotating duct with 90° ribs where they show that the Sherwood number ratio are 2.5 times higher than the fully developed values in a stationary smooth pipe due to the flow reattachment near the ribbed surfaces. They go on to show that there is enhanced mass/heat transfer in a higher aspect ratio duct because of the increased rib height-to-duct height ratio. However, the effects of turning region and rotation on mass/heat transfer become less significant with the increment of duct aspect ratio.

Investigations in the areas of rib roughed cooling, rib configurations and ribbed duct aspect ratios have been studied for several years. Literature review shows that there hasn't been any extensive research on CFD analysis for internal channel with rib

roughness giving ideal turbulence models which effectively match experimental conditions. This is because of geometrical constraints and complex flows within these cooling channels.

The fundamental objective for this research is to increase power output while increasing the efficiency of the gas turbine. Hence to increase the efficiency, it is important to maximize the heat transfer rates within the channels. Hence to model accurate computational models which mimic the flow conditions in a real gas turbine, it is extremely important to benchmark experimental results with CFD. This helps further investigations by reducing experimental costs and more accurate results. Hence investigating various industrial turbulence model is one of the goals for this study. Further objectives and goals will be discussed in depth in the next chapter.

3. Methodology and Set-Up

3.1. Introduction

The objective of this research is to highlight the different turbulence models for computation which are used to benchmark existing literature and experiments correlations. Using these computational setup, a geometry is made to replicate the experimental facility which is made in the Gas Turbine laboratory. Using these CFD results, the in-house experimental rig is validated. Fig. 3-1 below shows a schematic of the goals of what is done in this project.

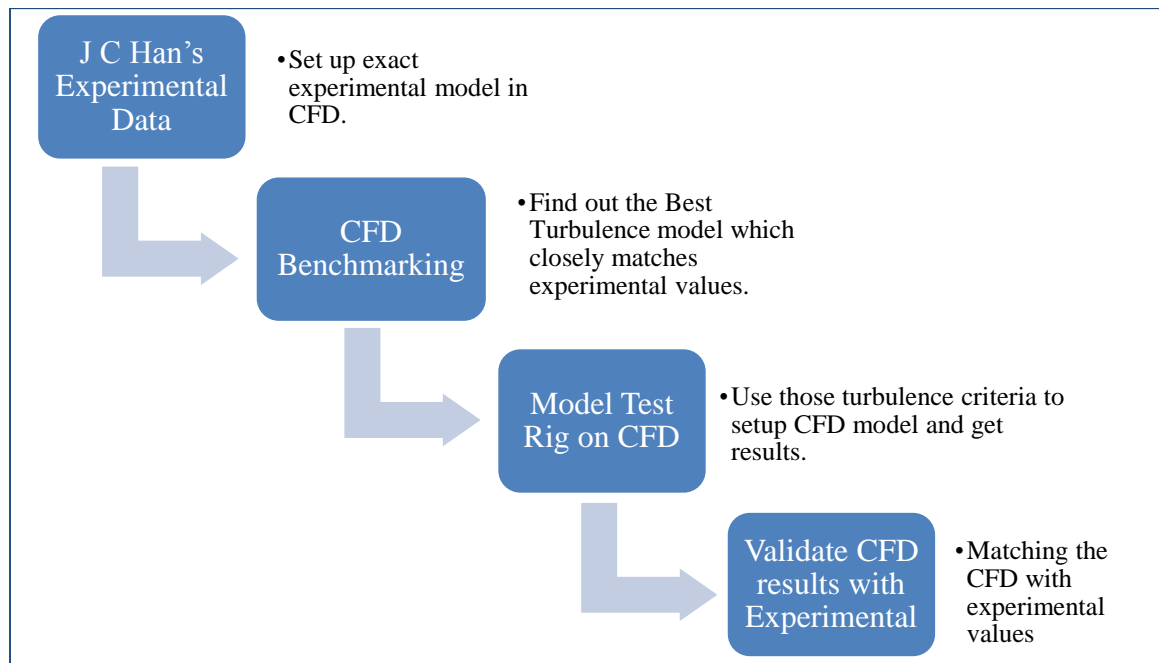


Figure 3-1: Flowchart of the goals of this project.

In addition to the experimental and CFD analysis of a single channel with periodic ribs, a study on smooth channel was also done experimentally as well as computationally in order to compare the enhancement of heat transfer when ribs are introduced.

3.2. Computational Setup

Numerical analysis were primarily conducted throughout this research but in order to design the complicated cooling configurations in a gas turbine blade to predict the different flow physics and heat transfer rates, Computational Fluid Dynamics was used as a vital tool. The advantages of using CFD is to visualize the 3D flow results compared to single measured points in experiments, which are more advantageous in designing efficient augmented heat transfer channels. In this thesis work, STAR-CCM+ was used for all CFD purposes including, building geometry, mesh generation and post processing data.

3.2.1. Computational Domain and Model Set-Up.

The computational model being setup is to replicate the experimental work done by J.C. Han, J.S. Park and C.C.Lei (1985). This study shows a computational validation in which experimental comparisons of various rib geometries seeing a range of different Reynolds number. Fig. 3-2 below shows the basic characteristic lengths for the rig and the non-dimensional units for the ribs.

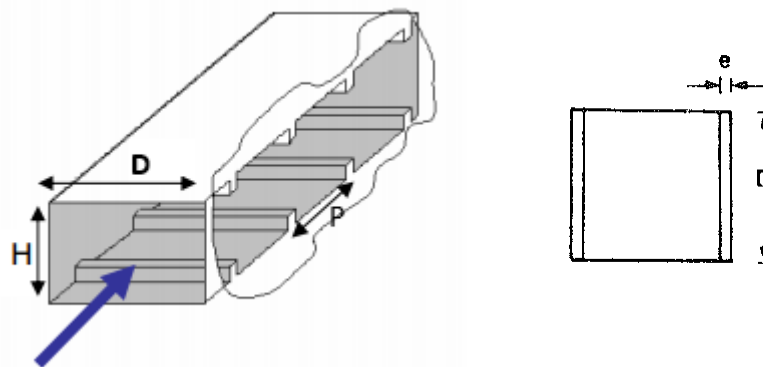


Figure 3-2: Various geometric parameters of the channel (Han, 1985).

The model setup for this case in particular is a rib roughed surface with periodic ribs on both sides. The whole setup is 3.048 m long consisting of 2 major sections, an unheated inlet duct which is 1.524 m long followed by another same sized channel which has heaters installed in them providing a constant heat flux on the bottom walls with ribs. The duct was a square with 0.076 m side. The rib size and spacing was non-dimensionalized with a rib pitch-to-height ratio of $P/e = 10$ and rib height-to-hydraulic diameter of $e/D = 0.063$. This ended up giving a square rib of side 0.00476 m. Fig. 3-3 below gives the channel setup which was replicated from Han's (1985) work.

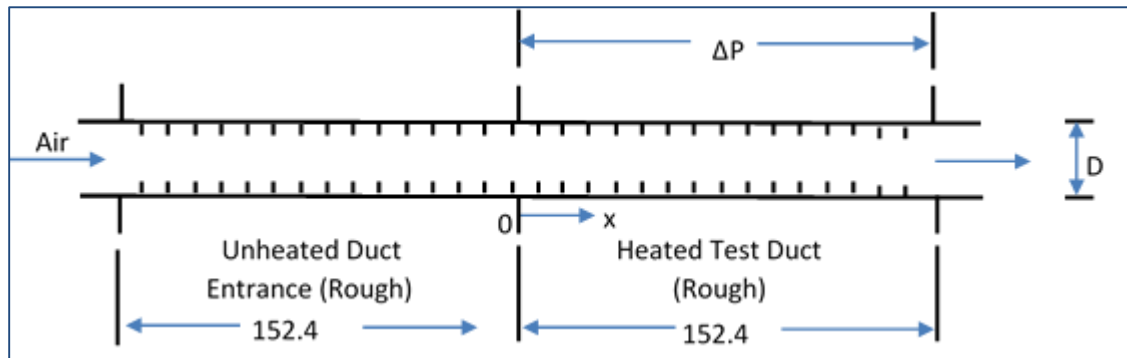


Figure 3-3: Representation of the channel setup.

The reason to put ribs on both sides of the wall was to increase the heat transfer between the walls as both the top and bottom wall are in contact with the hot main fluid flow on the outside. Hence ribs on the opposite walls increase the heat transfer within the channel extracting more heat. The heat transfer coefficients were calculated with a T_{ref} which is the local mean bulk temperature, calculated using the energy balance. The Reynolds number was calculated based on the inlet velocity, local fluid properties and hydraulic diameter.

To eliminate any discrepancies in setting up the computational model, the geometry was created at full scale. To simplify the computation, a symmetry plane was made on the top wall to duplicate the ribs and also another symmetry plane on one of the side walls hence modelling only one quarter of the actual rig. This can be seen in Fig. 3-4 below.

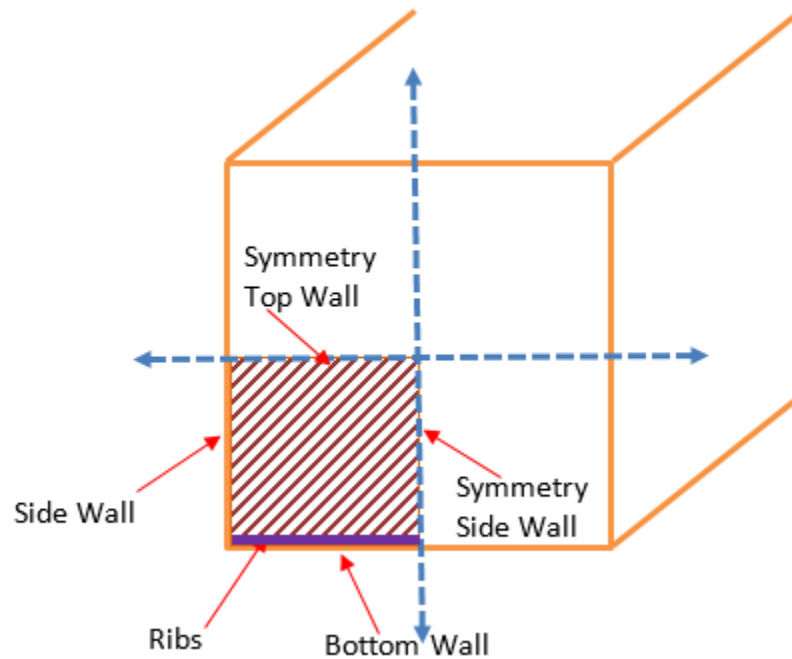


Figure 3-4: Section modelled in CFD

The domain was set up with 2 section each having 33 ribs on the bottom wall. The flow rates were established using a velocity inlet at the entrance, a transition between the outlet of the unheated duct to the inlet of the heated duct and then a pressure outlet at the exit. A field function was created at the inlet in order to match a Reynolds number of 21,500 which resulted in a velocity of 4.452 m/s. The heated section of the rig has a constant heat flux which helps give variation in temperatures through the rig. The heat flux was set at 1650 W/m². The case analyzed in this study is a 90° case where the ribs

are perpendicular to the main fluid flow. Fig. 3-5 below gives the domain which is set up in STAR-CCM+ Ver. 9.02.007. In the picture the top and the side symmetry walls have been hidden to show the internal section of the ribs.

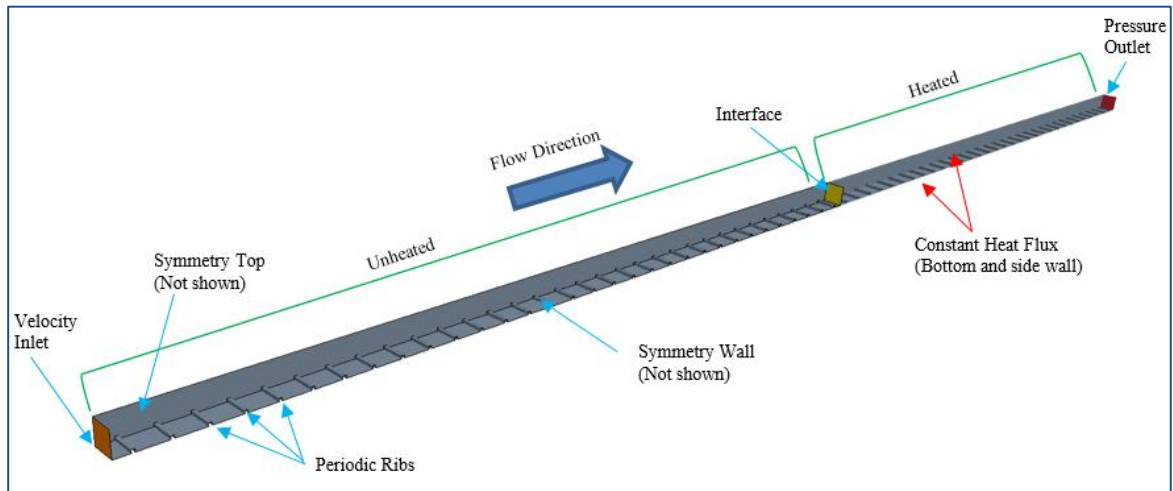


Figure 3-5: The Domain Set-up

3.2.2. Meshing and Turbulence

The mesh setup changed with the relevance of the part and its role in heat transfer - the ribs and the bottom wall were finely meshed whereas the side walls were kept coarser. This was done keeping in mind that there is no drastic change between the cell sizes in both regions. Polyhedral elements with prism layers and a surface wrapper mesh types were used to capture the normal temperature gradient and the boundary layer effects. The mesh size in the finer region was set to 0.6 mm polyhedral elements with 20 prism layers near the edges (2mm thick). The total cell count of the whole mesh summed up to about 29 million cells. Fig. 3-6 below shows the mesh transition of the 2 regions and also the mesh on and around the rib.

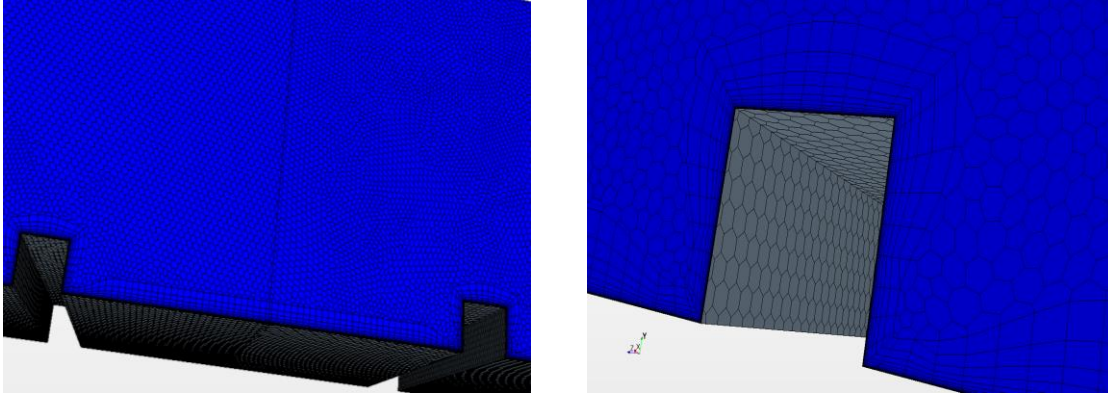


Figure 3-6: Mesh sizes and cell quality around the rib.

Mesh independence study was done by testing different base sizes in STAR-CCM+. A base size in STAR-CCM+ is defined as the setting the different values like surface minimum/target size, boundary layer thickness etc. proportional to the base value. Hence to refine or coarsen the mesh, only the base size needs to be changed which will automatically change the desired values. Mesh independence was obtained by running several cases at different base sizes. Fig. 3-7 below shows 3 cases with base sizes of 0.9mm, 0.6mm and 0.45mm giving a total cell count of approximately 7.9 million, 28.9 million and 56.4 million respectively. This total cell count includes both the unheated and heated surface of the computational rig. Surface average temperature and the average Nusselt number on the bottom wall were used to compare in these 3 cases in order to find the least difference. It was noticed in the figure that the change in temperature is 3.6% between the 0.9mm and the 0.6mm, but only 0.14% between the 0.6mm and the 0.45mm case. A similar trend is noticed in the Nusselt numbers as well, where its 6.2% between the first 2 cases and 0.12% between the second 2 cases. Hence using the second case with 0.6mm base size is more efficient since similar results were noticed without the need of a finer mesh. A mesh independent case is also important because it helps to judge the right

mesh size, which in return reduces the computation time. The mesh independent study was done for the Rk- ϵ turbulence model.

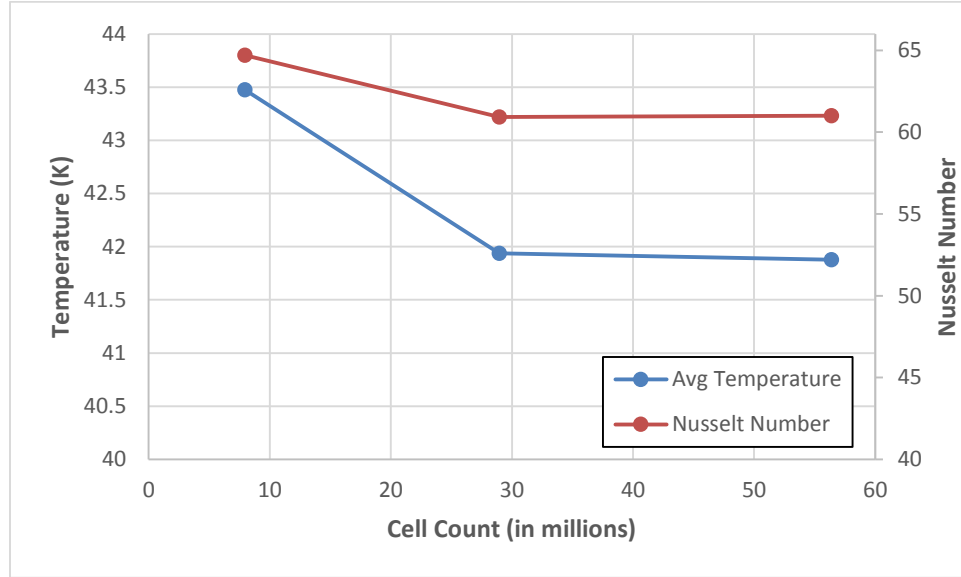


Figure 3-7: Avg. surface temperature and avg. Nusselt number vs. Cell count (Basesize)

Y_+ is the non-dimensional wall distance for a wall-bounded flow. It is used to capture wall effects within the boundary sublayer. Y_+ is given by the following equation:

$$Y_+ = \frac{u_* y}{\nu} \quad (2)$$

Where u_* is the friction velocity, y is the distance to the nearest wall and ν is the local kinematic viscosity of the fluid (CFD Wiki). Y_+ values are low for low Reynolds numbers. The Y_+ values on the heated walls were made sure to be less than one. The range of the Y_+ values were around 0.02 to 0.08. Fig. 3.8 and 3.9 give the Y_+ contours for the side wall and bottom ribbed wall respectively.

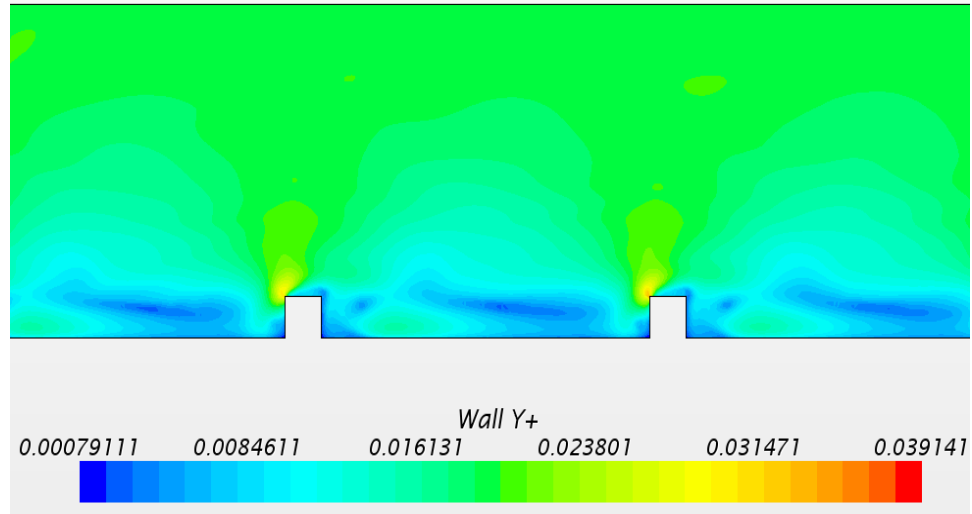


Figure 3-8: Y+ contour for the side wall.

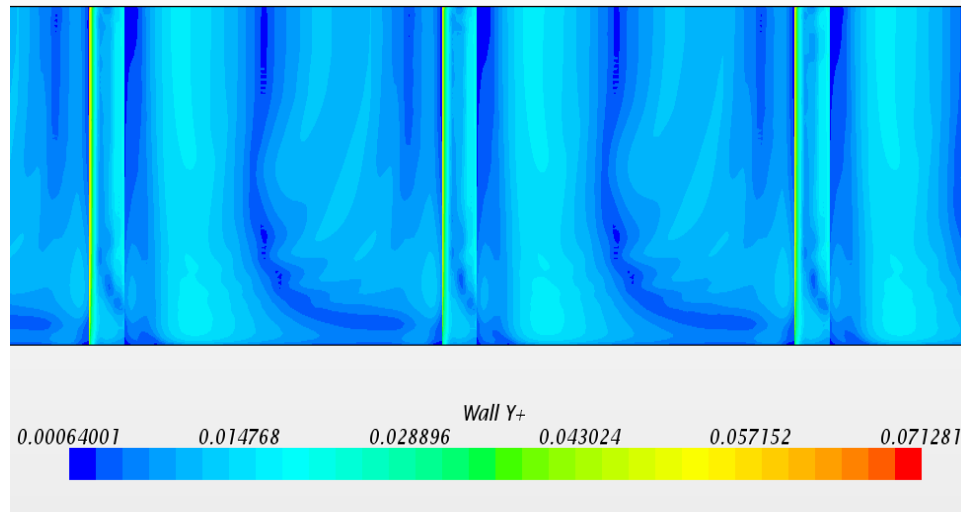


Figure 3-9: Y+ contour for the bottom ribbed wall.

The turbulence models being analyzed in this study are realizable k- ϵ , Menter's k- ω SST, the v^2 -f model and EB k- ϵ model. These turbulence models have been briefly being discussed below.

Realizable k- ϵ (rke): The R k- ϵ model is the most versatile and widely used 2 equation industrial turbulence model in internal channels. Even though the realizable k- ϵ is a better version of the k- ϵ model, it is still not that apt for flows near the end wall. Not

only is the realizable k - ϵ model an improvement of the standard k - ϵ model, but it is also very versatile and widely used turbulence model. The realizable k - ϵ model is a two equation model solving the Navier-Stokes equation for dissipation (ϵ) and kinetic energy (k) values through the turbulent region (STAR-CCM+ Manual). This is because near the viscous sublayer, the viscous forces are dominant over the turbulent forces due to which the turbulence effects are neglected. Standard k - ϵ is not capable to resolve the flows in that region hence the realizable k - ϵ model is better as it corrects for abnormal peaks in strain as well as accounts for compressibility and buoyancy (Davis, 2012). The realizable k - ϵ model is fairly reliable in various applications as a starting point to get initial results.

Menter's k - ω SST: The k - ω model is similar to the k - ϵ model except that it models the specific dissipation rate (ω). Menter suggested to blend the wall distance functions by adding a cross diffusion term near the wall whereas the k - ϵ in the free stream. This gave an effective blend of k - ω and k - ϵ models. Hence Menter's shear stress transport (SST) model is an improvement over the standard Wilcox model as it shows the sensitivity to the free stream conditions. This model is widely used in the aerospace field where the viscous flows are typically resolved and the turbulence models are applied throughout the boundary layer (STAR-CCM+ Manual).

V^2 -f: The v^2 -f model is also a variant of the k - ϵ model which includes two additional equations, namely the normal stress function and the elliptical function which more accurately predicts the effects of turbulence at the wall (Davis, 2012). Along with the near wall turbulence effects, it also predicts the non-local pressure-strain effects which is very crucial for accurate prediction of heat transfer, skin friction and flow separation.

Elliptic Blending k- ϵ (EB k- ϵ): Another variant of the k- ϵ model was proposed by Manceau and Hanjalic. This is one of the most robust models along with the *BL* V^2 - k model which is widely used for complex flow geometries. The EB k- ϵ model is also a more accurate in predicting the near wall effects compared to the standard version of the k- ϵ model. It is also more stable than the SST k- ω turbulence model.

3.3. Experimental Setup

Once getting the computational model for the rig ready on STAR-CCM+, the experimental test testing facility was built starting from a basic smooth channel. The objective was to have the experimental rig to first run with a smooth channel in order to get a baseline result for comparison. The test section was designed in such a way to incorporate two different configurations of turbine blade internal channel cooling i.e. impingement jet cooling and rib turbulated cooling. This test rig was designed to represent pressure and heat transfer tests on a single channel inside the turbine airfoil. There were several hurdles and issues which needed to be tackled before the rig could be properly functional but overcoming those problem helped the team better understand the working of different components.

3.3.1. General Rig Description

All experiments were carried out at steady state and constant heat flux on the target wall conditions. As mentioned before, the test rig was built to incorporate two different testing configurations. The test rig was build using $\frac{3}{4}$ ' acrylic plates with a width of 12 cm and a total length of 1.5 m. Fig. 3-10 below shows the geometry of the test section.

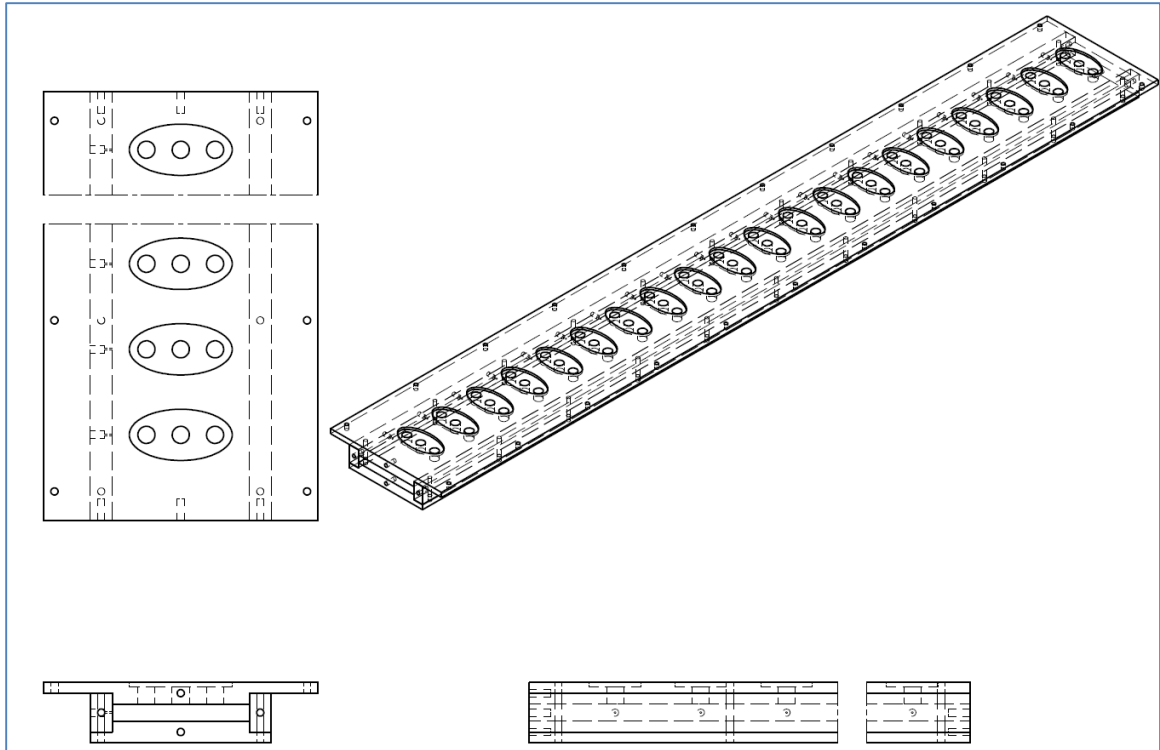


Figure 3-10: CAD model for the experimental rig test section

The rig was attached to a centrifugal blower using PVC pipes on one end and was kept open on the other end for the air flow to enter the test section. The suction side of the blower was used so that the atmospheric air was drawn through the open end of the channel into the blower. The air being sucked into the blower was controlled and the flow rates were measured using a venturi type flow meter. These venturi flow meter readings were used to calculate the average channel Reynolds number. Flow control valves help monitor how much flow is sucked into the blower. Auxiliary valves are used to balance the flow in order to not work the blower too hard. Fig. 3-11 below shows the experimental blower used with its piping configuration.



Figure 3-11: Experimental blower used with control valves.

The side walls were screwed to the top and bottom plate using threaded studs and all joints were made leak free by sealing them with a Teflon gasket. Fig. 3-12 below shows the flow loop of the experimental test rig where the atmospheric air is sucked into the test section from the cross flow inlet. This flow then passed through the test section with either the smooth channel configuration or the ribbed channel configuration.

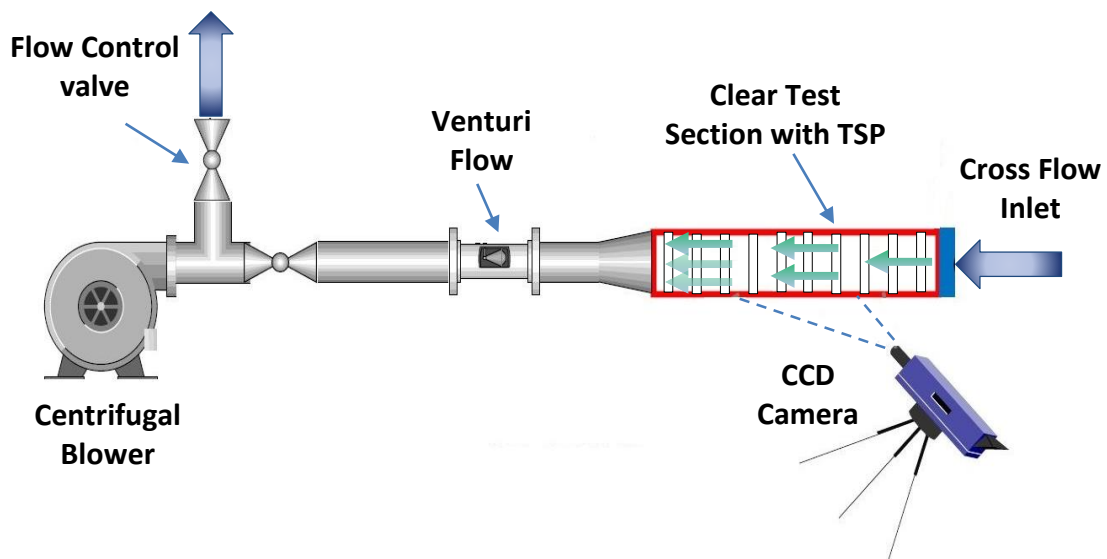


Figure 3-12: Flow loop of the experimental rig

One of the side walls were equipped with static pressure taps used to get pressure profiles along the length of the test rig. The target wall which is the bottom wall was painted using Temperature Sensitive paint (TSP) and was then instrumented with Inconel (Grade 625) heaters constructed from a series of single heater strips each 15mm in width. Each of these heaters were connected in series which provided an overall high resistance. These heaters were stuck onto the bottom wall using double sided Kapton tape. These heaters were powered with a VariAC which kept a constant heat flux on the bottom wall through the test section. Along with the TSP, the temperature readings were verified using type T thermocouples placed on the bottom wall of the rig at various lengths. The bulk temperature was also measured using a type T thermocouple at the end of the test section. Fig. 3-13 below shows the arrangement of the strips on the bottom wall.

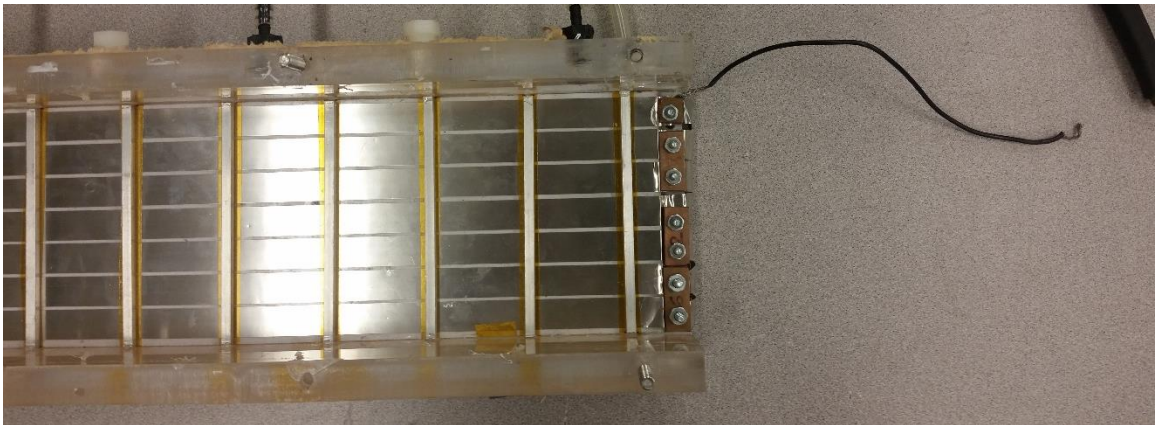


Figure 3-13: Arrangement of the heater strips on the bottom wall

While running the heat transfer experiment, the TSP was excited using 2 kinds of LED (Light Emitting Diodes), one custom made series of LED light bulbs and the other being a high powered LED spot light. In order to not have a single spot of light from the LED lights, a reflector sheet was used to evenly distribute the lights. Tests showed that it takes an approximate of 15 minutes for the intensity of the lights to stabilize. Once excited, the images to calculate the heat transfer rates were captured using a scientific grade single CCD (Charged Coupled Device) thermos-electrically cooled camera (PCO edge) with a Nikon zoom lens. This camera was placed on a 3 axis traverse which helped position the camera to take the pictures at the appropriate distance. This traverse was programmed on Matlab to move in the positive and negative, X, Y & Z direction. The traverse was needed to help move the camera along the test rig due to the very small area captured by each image. Hence 2 images were captured, one upstream and one downstream to cover the full span of the test rig. These images were then processed in Matlab and stitched together in order to get one single image.

In order to prevent the TSP from being degraded by exposure to regular lights, a dark room was constructed using 80-20 bars and cloth. Fig. 3-14 below shows the setup for the camera, traverse, LED lights as well as the test rig in the dark room.

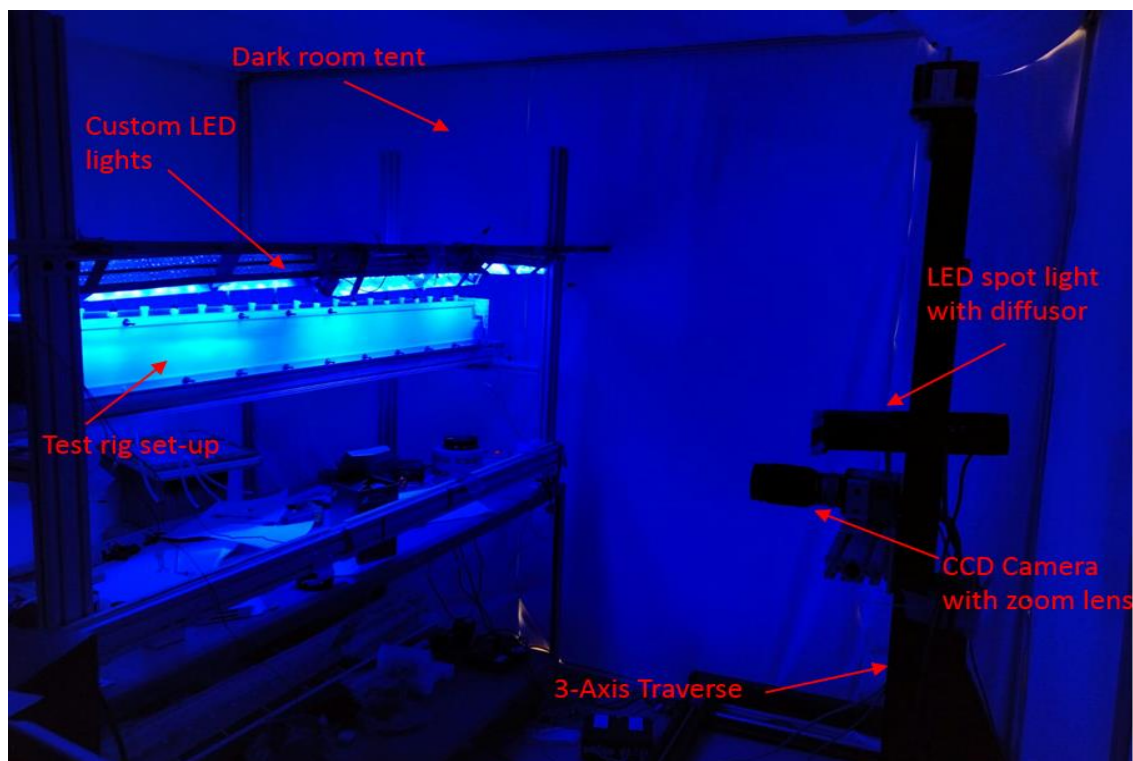


Figure 3-14: Test rig set up along with LED, Camera, and Traverse in the dark room

Uni-Coat TSP from ISSI Inc. was used for the experimentation of this lab. The TSP comprises of luminescent paint mixed with fluorescent molecules and a binder. These molecules when excited with the proper wavelength, undergo a reaction which is sensitive to temperature. This change is captured using a specific camera. Once the images are obtained, they are then processed to get the full temperature distributions along the full length of the TSP paint applied. The TSP is a highly reliable mode of measure temperature changes compared to having multiple thermocouple on the surface which is being tested. Before being used, the TSP needs to be calibrated. This was done by painting a small block of acrylic which was then glued to a constant temperature copper block. The temperature of this block was controlled by the voltage supplied to it.

Pictures were taken before and after heating the block. These images are then converted into intensity ratios to calculate the change in heat transfer from the cold to the hot image. Using these calibration values the Matlab code is written which is used to process the intensity images captured from the camera. Fig. 3-15 below shows the bottom wall of the test section painted with TSP.

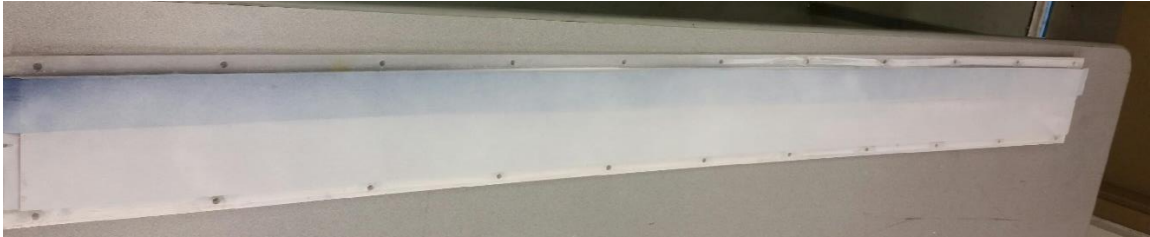


Figure 3-15: Test section bottom wall painted with Temperature Sensitive Paint.

3.3.2. Ribbed Channel Setup

The experimental test rig for the ribbed configuration was set up in the same smooth channel with the addition of ribs to the top and bottom surface. It followed the same Pitch-to-rib height (P/e) of 10 as in the CFD analysis but the rib height-to-Hydraulic diameter (e/D) was increased from 0.063 to 0.076. This e/D resulted in having square ribs with a cross section of 5 mm. Long aluminum 6061 bars were cut to make the ribs of desired length. According to the selected pitch, the ribs were placed 45mm apart which added up to a total of 32 ribs along a 1.55m test rig. These ribs were stuck onto the heater strips using Kapton tape. Additional adhesive was used on the ends of the ribs to make sure they were glued into place as well as are adhered to the side walls. Fig. 3-16, 3-17 below shows the ribbed test setup for the bottom and top wall.



Figure 3-16: Ribbed channel test rig setup - Bottom wall



Figure 3-17: Ribbed channel test rig setup - Top wall

3.4. Data Reduction

Data reduction was conducted multiple times during the testing process to evaluate values to be compared. Flow velocity through the channel were calculated to evaluate the boundary conditions at the wall, friction factor calculations to differentiate the pressure profiles and finally the heat transfer calculations were don't to compare Nusselt number values.

A pitot static tube and a boundary layer probe was used to evaluate the velocity profiles along the span wise direction of the test section at various locations. The pitot static tube gave total and static pressure values, the difference of which gives the dynamic pressure. Using this dynamic pressure, the velocity of the flow can be calculated. This is represented in the following equation.

$$p_s + p_d = p_t \quad (3)$$

$$P_s + \frac{\rho v^2}{2} = P_t$$

Hence we get velocity as:

$$v^2 = \frac{2(P_t - P_s)}{\rho}$$

The pressure correlations to compare smooth channel and ribbed channel data was done using the Fanning friction factor. This determines the amount of extra work needed to be done to obtain these high heat transfer coefficients. The Fanning friction factor was calculated for the heated section which is assumed to have a fully developed flow with the channel. The friction factors were averaged between the smooth side and the ribbed side using the formula given below:

$$\bar{f} = \Delta p / [4 \left(\frac{L}{D} \right) \left(\frac{\rho v^2}{2g_c} \right)] \quad (4)$$

Here g_c is the conversion factor for the maximum center line velocity for ribs (Han, 1985).

In case of the heat transfer calculations, it was fairly straight forward since all the simulation and experiments were ran at steady state. In case of the ribbed configuration, lateral conduction was assumed to be treated as a case of an adiabatic pin. Hence with the help of the wall surface temperature, the reference temperature and the heat flux generated by the heater strips, the heat transfer can be calculated. In case of experimental data reduction, Matlab was used to calculate the heat transfer and Nusselt number values due to the fact that every pixel of TSP data gave an intensity value (and hence a

temperature value).

To evaluate any heat loss within the channel, the whole test section was filled with insulation so that there is no room for any heat leak. Once insulated, the power input were recorded to reach the desired operating temperatures. Minor losses were accounted for due the low conductivity of acrylic walls. The reference temperature for the heat transfer was calculations was recorded as the bulk temperature for all cases.

It was determined that the high resistance of the heater strips had minimal thermal effects on to the channel. Hence the total heat flux from the heaters generated was calculated using:

$$q'' = \frac{V^2}{R_h * A_h} \quad (5)$$

Where V is the voltage across each strip measured using a digital multimeter.

Hence the effective heat flus is given by:

$$q''_{eff} = q'' - q''_{loss} \quad (6)$$

Thus the heat transfer coefficient can be determined by the following formula:

$$h = \frac{q''_{eff}}{T_w - T_r} \quad (7)$$

And the Nusselt number relation is given by:

$$Nu = \frac{hD}{k} \quad (8)$$

4. Results and Analysis

4.1. Smooth Channel Validation (Experimental)

The velocity profiles for the smooth channel were performed using both the pitot static tube as well as the boundary layer probe. These results were then compared to a CFD simulation as well to validate the rig. These velocity readings were taken in the fully developed region. The main goal for this validation was to determine the flow conditions in the boundary layer close to the wall which is shown by the gradients in Fig. 4-1.

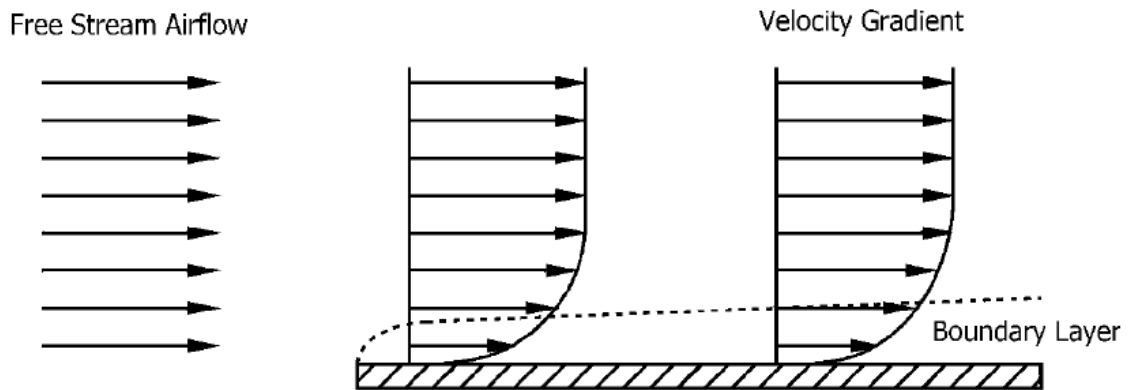


Figure 4-1: Velocity profiles at the boundary layer (Chklovski).

Expecting similar profiles, the velocity profiles for a Reynolds number of 75,000 is plotted in Fig. 4-2. The pressure measurements were taken span wise along the centerline of the test section. As seen in case of the CFD and the pitot static tube, the velocity profile were taken only for half the channel span and then duplicated since they have a symmetrical profile. It is observed that the Boundary layer probe closely matches the computational results since the boundary layer probe is more accurate predicting the near wall effects better than the Pitot tube. Moreover this helps validate the computational results by stating a fine mesh at the near wall hence resolving the boundary layer accurately.

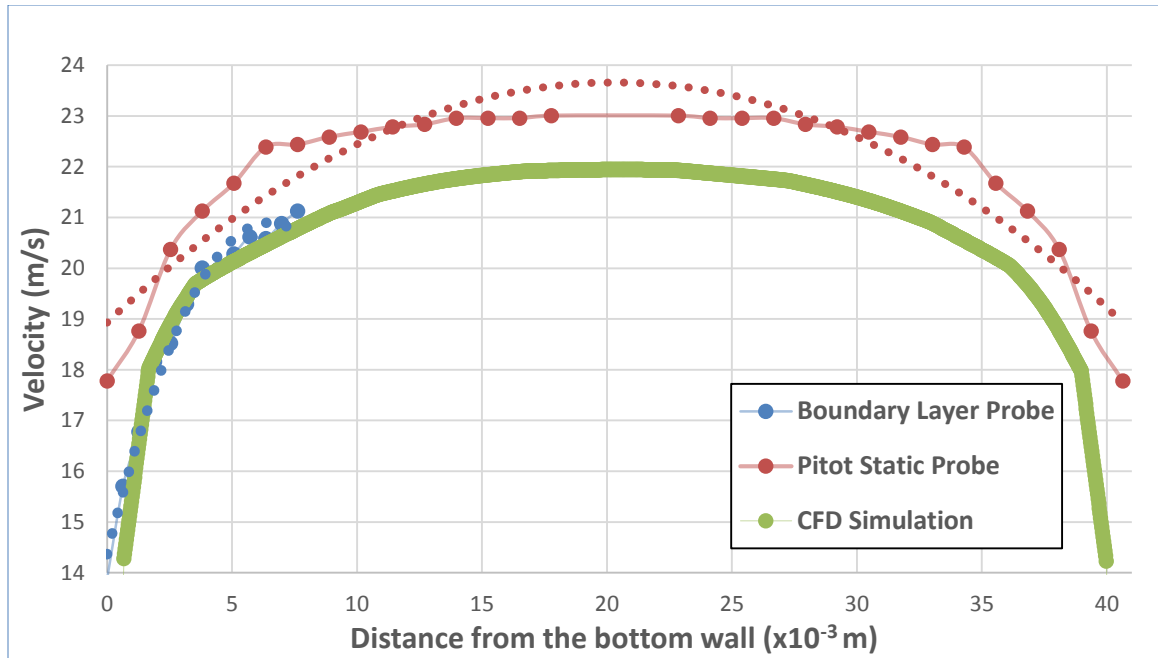


Figure 4-2: Experimental vs. CFD Velocity profiles.

4.2. Ribbed Channel Benchmarking (CFD)

CFD analysis is done in order to deeply investigate the flow physics of the complex flows inside the channels. CFD is carried out to check the legitimacy of the experiments ran even though a lot of times it does not yield the most accurate results. Mentioned earlier, the first step towards the goal of this thesis is to setup a smooth channel case in STAR-CCM+ to computationally analyze the basic results.

4.2.1. Benchmarking to JC Han

The goal of this section is to benchmark the experimental data from JC Han et al. (1985) work with various computational models in STAR-CCM+ by replicating the experimental conditions. By doing so, the best turbulence models were found which closely matched the published values. The CFD model was set up as a $\frac{1}{4}$ th structure by

setting the top and one of the side walls as a symmetry plane which duplicated the results through the rest of the model. By doing so, the computation time and resources were reduced. All these simulations were run on the ERAU Rigel network, typically taking 24 hours for an average of 15,000 iterations. Fig. 4-3 below shows the residuals for the iterations averaged over time for the EB k- ϵ turbulence model.

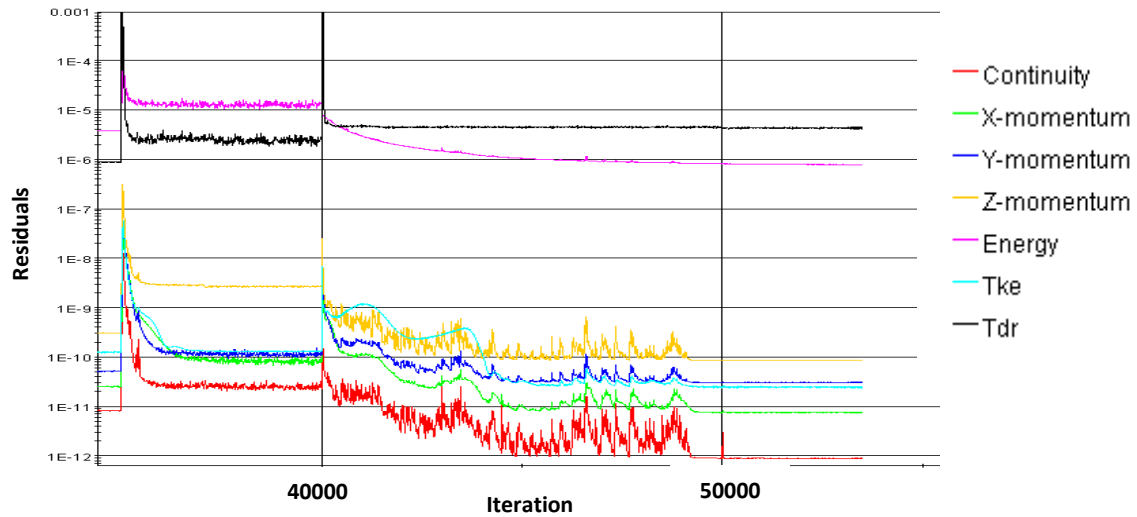


Figure 4-3: Residuals for time averaged iterations.

4.2.1.1. Pressure Data and Friction Factor

Before jumping onto understanding the heat transfer analysis of the rib effect on the cooling of the turbine blade, it is important to analyze the fluid flow characteristics. The ribs are intended obstructions to the flow so not only is it important to study the turbulence caused, but also to see the how much loss in pressure is needed to drive the flow through the channel.

Pressure comparisons between experimental results and computational results were made using the friction factor. Fanning friction factor is a dimensionless quantity which is used to describe frictional losses through the channel. These losses are different

for different turbulence models and the Reynolds number at which the channel sees the flow.

As seen in Fig. 4-4, the friction factor for Han's (1985) data at $\alpha=90^\circ$ is compared with smooth channel results as well as the present study for the four different turbulence models. The four different turbulence models were ran at a Reynolds number of 21,500 whereas only the R k- ϵ , EB k- ϵ and the k- ω model was ran at 42,000 Reynolds number. This was because the V^2f turbulence model is very unstable at higher Reynolds number and diverges. It is to be noted that the friction factor for the smooth channel sees a constant rise with increased Reynolds number.

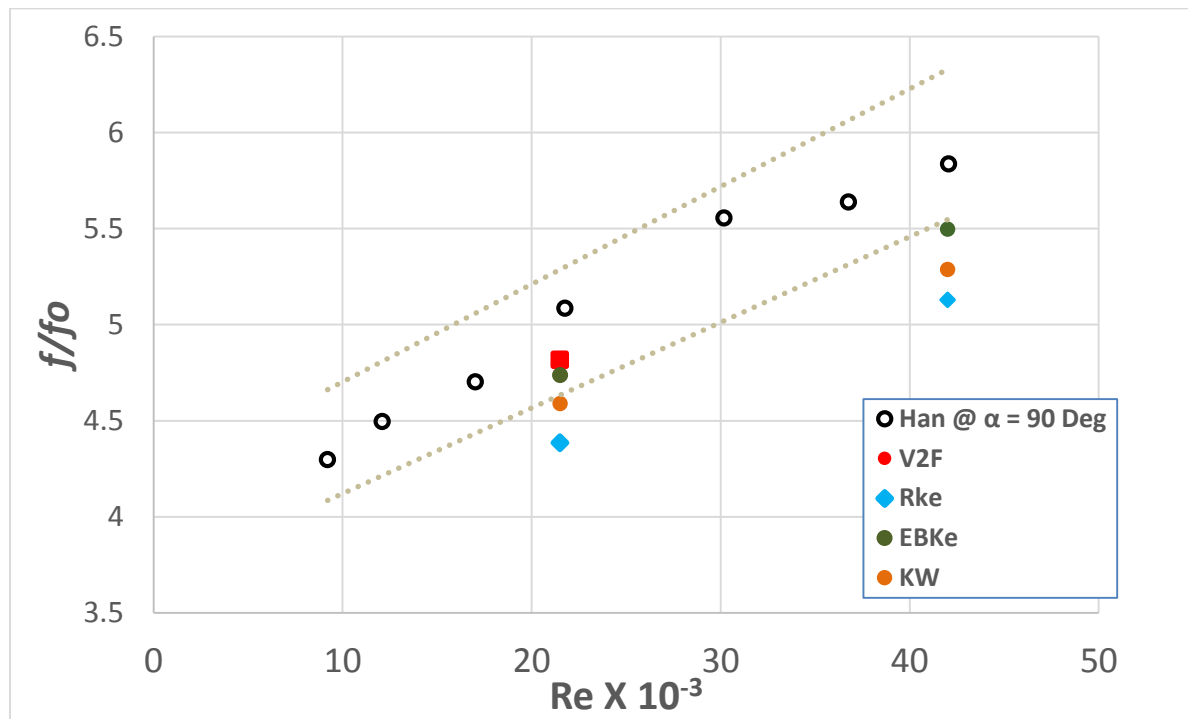


Figure 4-4: Friction factor for varied α experimentally compared to CFD at $P/e = 10$

It is seen that the friction factor for Han's (1985) data is almost constant with different Reynolds numbers. The friction factor ranges from 4 to 6 times the smooth

channel values which shows a linear loss in pressure across the channel. As seen in the figure, with increase in Reynolds number, the friction factor increases due to increased turbulence which callused higher pressure drops. Table 4-1 below gives a percent difference between the friction factors got experimentally by JC Han to the computational models.

Table 4-1: Friction factor comparison to Han's (1985) data (Percent Diff.)

	Re = 21,500	Re = 42,000
V ² F	5.3%	-
R k-ε	13.8 %	12.1 %
EB k-ε	6.8 %	5.8 %
k-ω	9.8 %	9.4 %

As highlighted in the table above, the V2f model predicts the closest to the experimental value for Re @ 21,500 and EB k-ε matches closest at Re @ 42,000 which are within the uncertainty of 6.8% according to JC Han's data.

4.2.1.2. Heat Transfer Analysis

To analyze the different turbulence and compare them, Nusselt number variations were compared along with results from Han's (1985) work. Figs. 4-5 and 4-6 give the Nusselt number contour plots of the fully developed section for the EB k-ε and V²F steady-state, mesh independent model. As it can be seen, the EB k-ε shows a better near wall prediction than V²F model. Hence as seen before, it shows higher heat transfer. Than V²F. It is also noticed that V²f shows a significant drop in Nu. Even though the Nusselt numbers vary from model to model, it had a similar trend.

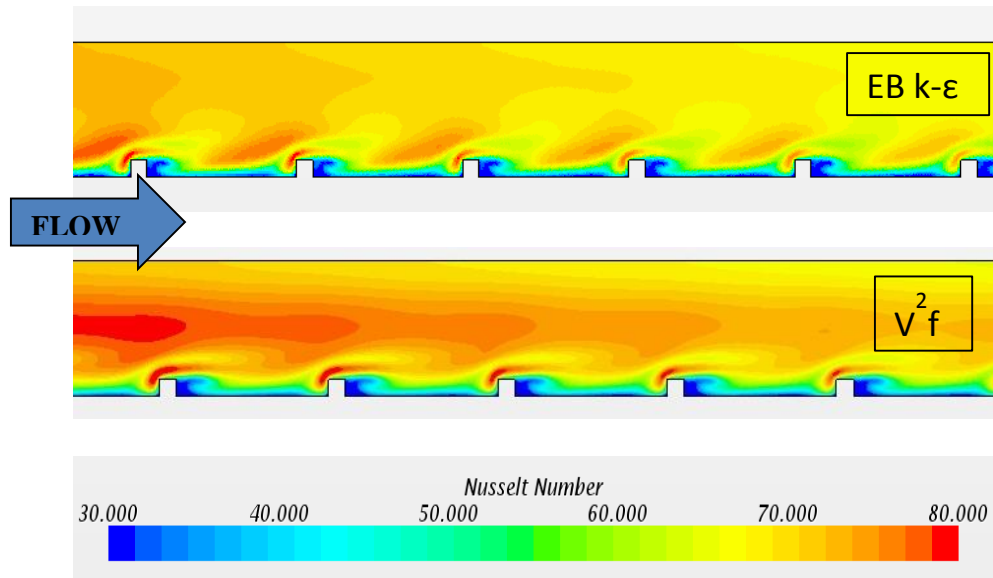


Figure 4-5: Nusselt Number contours for EBKe and V2F models on the side wall

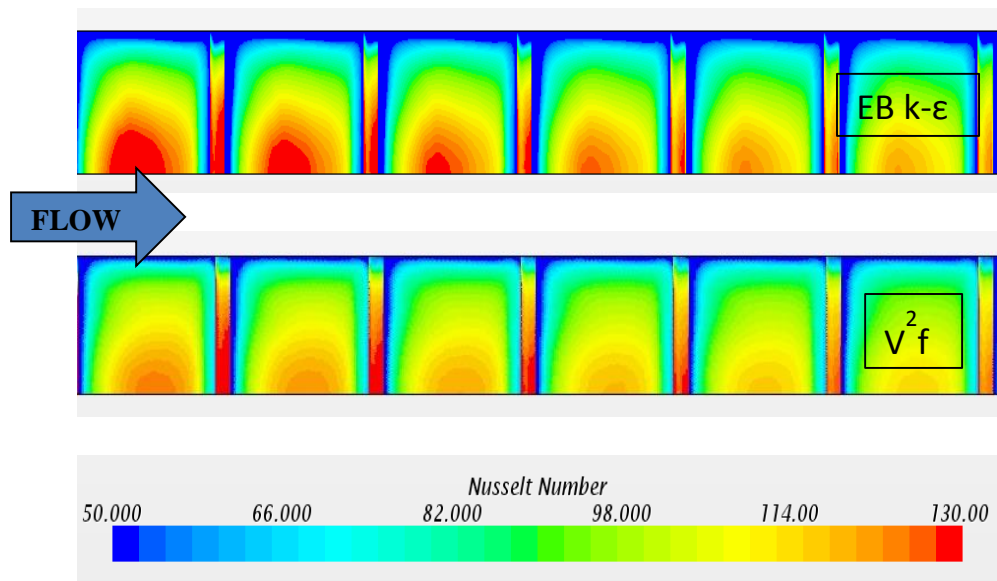


Figure 4-6: Nusselt Number contours for EBKe and V2F models on the bottom wall

As expected, the contours show a high Nusselt number on the top of the rib followed by a drop in Nu right after the rib. This is where the flow separates from the main turbulent flow. The region behind the rib has a very low Nu because of the flow reversal. The region between the two ribs also see high Nu values as the main fluid flow

is in contact with the hot gasses outside and hence it experiences the highest heat transfer.

The different turbulence models were ran on the most mesh independent case in order to extract data and analyze it. A derived presentation grid was made on the bottom wall as well as the ribs to generate Nusselt number values on them. They were then plotted along the length to get a Nu variation plot. In order to clean the plot and compare values with other turbulence models, a Matlab code was written to span average the values along the length. Fig. 4-7 shows the plot of the Nu vs. length scale (X/D) of the heated portion of the rig at two locations, the bottom wall and the rib plane. X/D is the non dimensionalized value of the distance in the X direction by the hydraulic diameter.

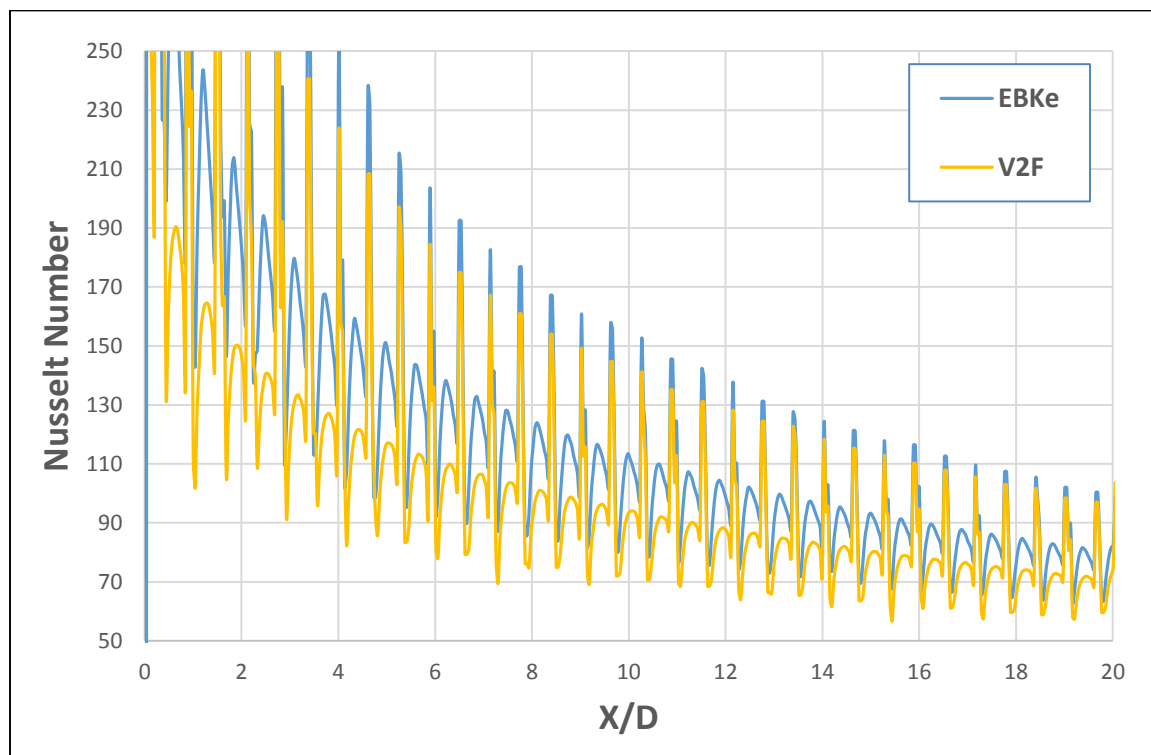


Figure 4-7: Span averaged Nusselt number variation on the Ribs

Regarding the variation on the ribs plane, it is seen that the EB $k-\epsilon$ turbulence model has very high Nusselt numbers in the starting few rows of ribs but going

downstream, it becomes linear and periodically fully developed. The V^2F turbulence models also follow a similar trend as the EB $k-\epsilon$ but have lower Nusselt number values. In the figure, the spikes show the Nusselt number on the rib surface whereas the plateau region gives the Nu in between the ribs.

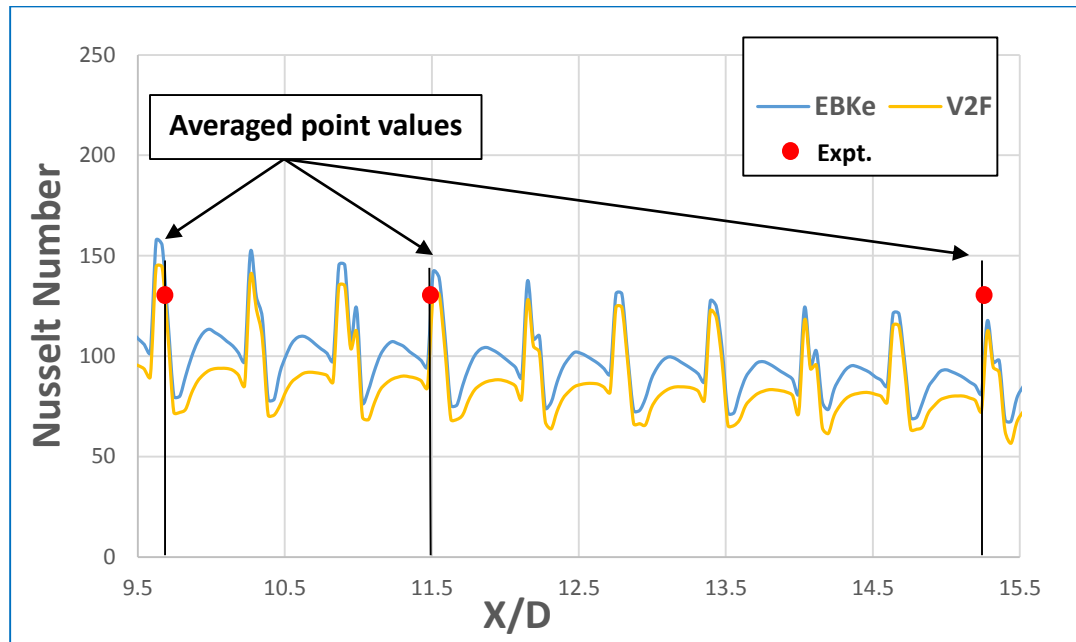


Figure 4-8: Fully developed region for Nusselt number variation (Zoomed In)

Fig. 4-8 shows a zoomed in region of the fully developed region. It displays the span-wise averaged Nusselt numbers between X/D of 9.7 to 15.3. The Average of the 3 locations in the fully developed region were compared to Han's (1985) work. The $k-\omega$ and EB $k-\epsilon$ matched the closest by over predicting by 2.5% and 1.6% respectively. On the other hand, the R $k-\epsilon$ and V^2F models under predicted by 7% and 4.7% respectively. These values fall close to Han's (1985) uncertainty of 6.8%. It is seen that all the three variations of the $k-\epsilon$ model give better results than the realizable $k-\epsilon$ model since they accurately account for near wall effects.

In the fully developed region, local Nusselt numbers were found by using point probes between an X/D of 9.7 - 15.3. This corresponded to 0.74m to 1.16m of the entire length of the channel. It is seen that the Nusselt number for the smooth side is lesser than the ones obtained at the ribbed surface. Fig. 4-9 below gives the distribution of the Nusselt numbers compared to Han's (1985) data in the fully developed region.

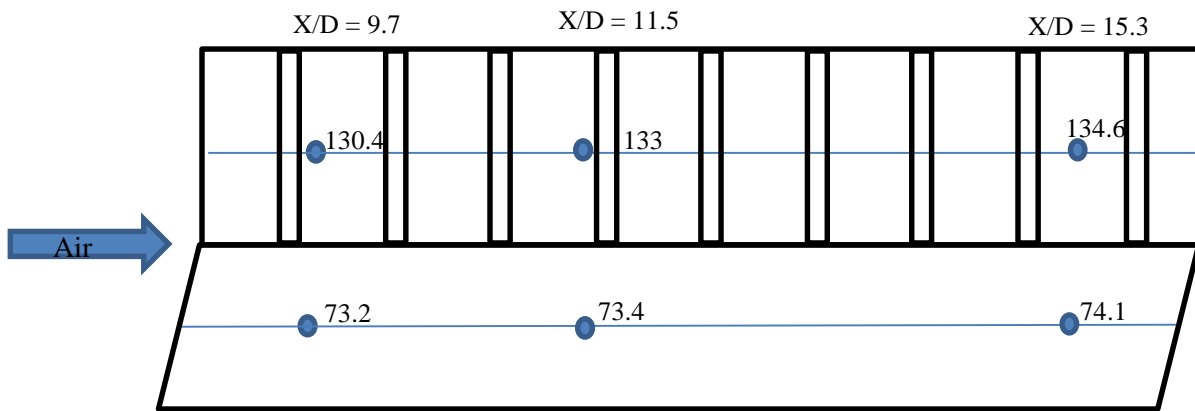


Figure 4-9: J.C. Han's Local Nusselt number values for $\alpha = 90^\circ$

Table 4-2: Local Nusselt number comparison between experimental & CFD models

	X/D	9.7	% Error	11.5	% Error	15.3	% Error
Rk-ϵ	Rib	119.5	8.4	110.2	15.5	105.7	18.9
	Smooth	63.3	13.5	58.9	19.5	57.3	21.7
EBk-ϵ	Rib	128.1	1.8	121.9	6.5	115.6	11.3
	Smooth	71.9	1.8	71.2	2.7	65.6	10.4
V²F	Rib	128.1	1.8	122.9	5.8	119.5	8.4
	Smooth	78.7	-7.5	74.9	-2.3	72.8	0.5
K-ω SST	Rib	124.2	4.8	119.5	8.4	110.2	15.5
	Smooth	68.0	7.1	63.3	13.5	62.9	14.1

Fig 4-10 below shows the flow visualizations displaying the velocity contours on the side wall and the Wall Shear Stress on the bottom wall. As it can be noticed, the blue

section shows where the recirculation zone ends and hence showing the reattachment length. According to literature, a reattachment length of 0.625 of a pitch is typically seen. So comparing it to the EB k- ϵ and V^2f model, the V^2f model closely matches literature but on the other hand, the EB k- ϵ model, even though it has a shorter reattachment length, shows a higher Nusselt number.

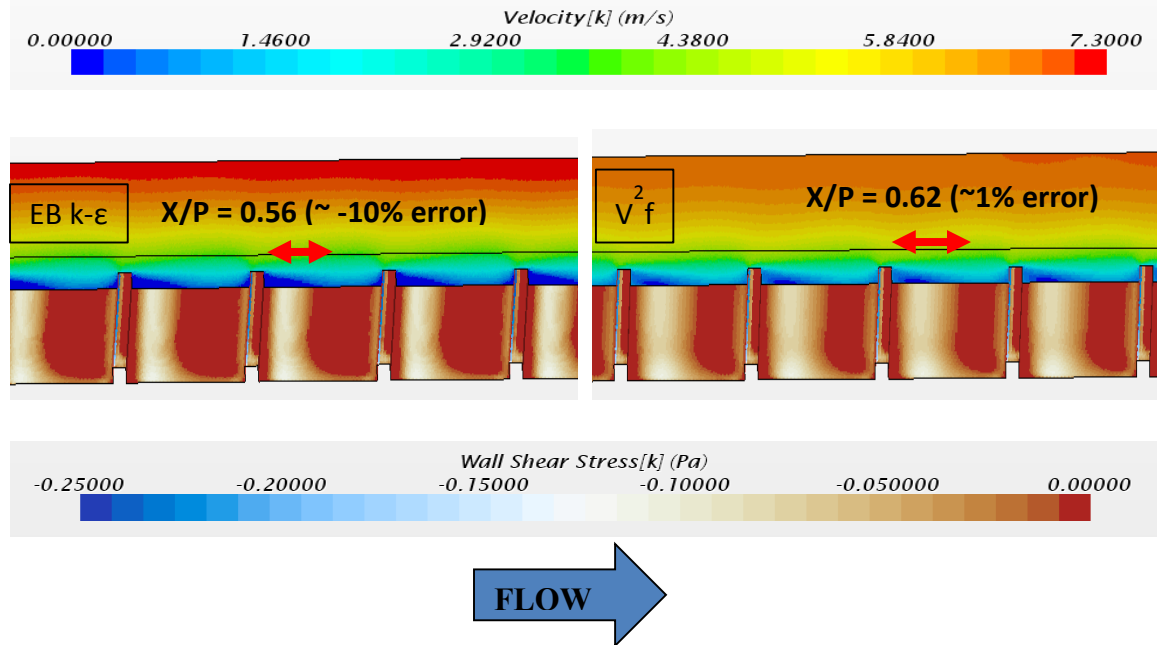


Figure 4-10: Velocity and Wall Shear Stress contours showing the reattachment lengths for EBke and V^2f .

4.3. PTML Ribbed Channel Data

4.3.1. CFD Analysis

After analyzing the results from the computational benchmarking, there were two turbulence models, V^2f and EBk- ϵ which closely matched the experimental values within the uncertainty. It is very difficult to judge which model fairs better than the other since both of them are within uncertainty. But going off the numbers, the V^2f showed the closest match at lower Reynolds numbers but struggled for numerical stability at higher Reynolds numbers, it also showed better matching in reattachment length. Thus for

preliminary analysis, the EBk- ϵ model was used to setup the CFD model for the in-house validation for the experimental facility. The experimental test rig was replicated into STAR-CCM+ and was simulated at a Re of 21,500 and 42,000 with the same boundary conditions.

Fig. 4-11 below compares the span averaged Nusselt number values on the bottom wall for a test section at Re of 21,500 and 42,000. It is noticed that the Nusselt number variation in both the cases decreases through the length of the channel. In case of the lower Re, it sees less variation in between the ribs. This is observed due to the less turbulence caused. Whereas for the higher Re, the Nusselt number peaks right at the leading edge of the rib and sees a low heat transfer rate behind the rib. Both these cases were compared to theoretical smooth channel values calculated by Dittus-Boelter and Gnielinski and it was observed that the ribbed channel gave a Nusselt number about 3 times of that which was seen for a smooth channel.

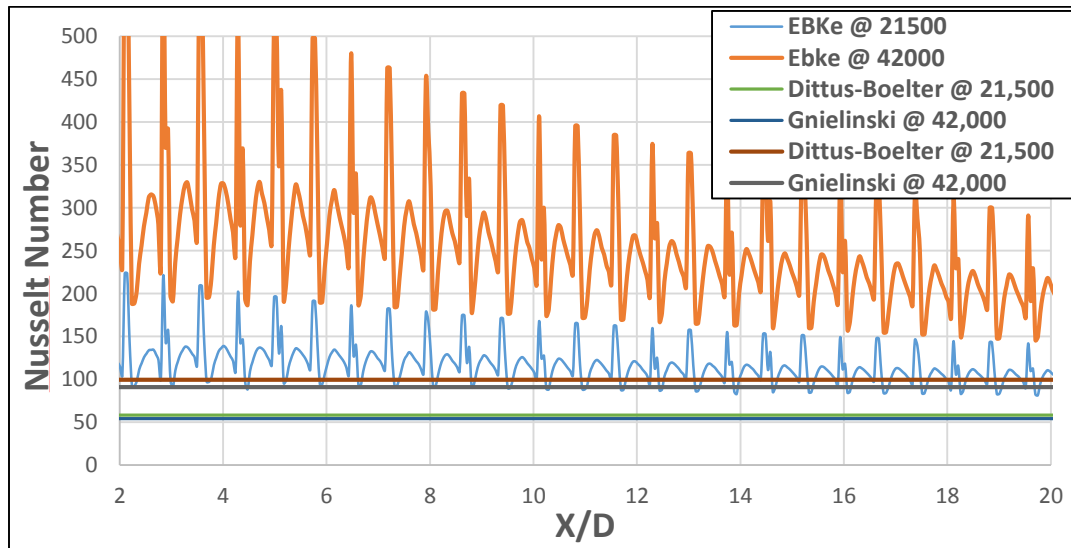


Figure 4-11: Computational span averaged Nusselt Number along the bottom wall.

Fig. 4-12 below shows the Nusselt number contours in case of the ribbed configuration for the EBk- ϵ model ran at a Re of 21,500. It is to be noted that in case of

the CFD simulations, lateral conduction wasn't taken into consideration hence the contours show a lower Nu at the side walls.

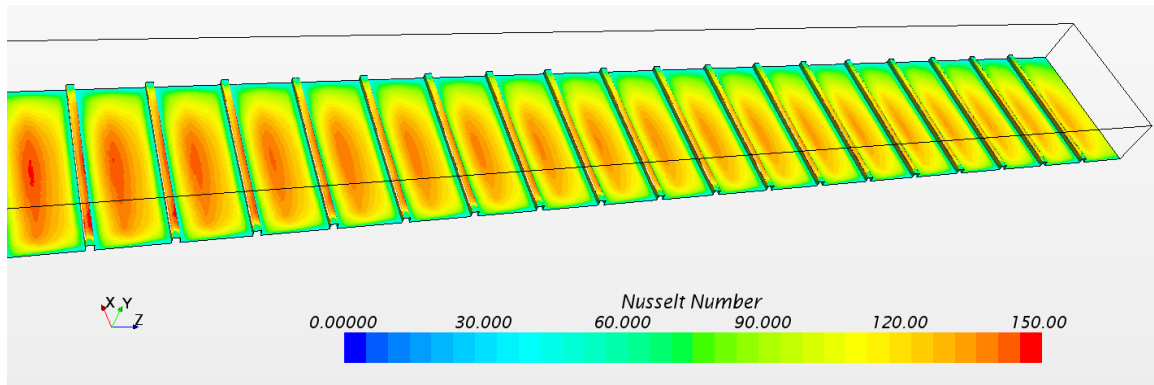


Figure 4-12: Nusselt number contour for EBk- ϵ model at Re of 21,500.

4.3.2. Experimental Analysis

The experimental analysis of the test rig was ran for 6 different cases. Two Reynolds numbers of 21,500 and 42,000 were analyzed at 3 different heat fluxes of 566, 1670 and 2055 W/m². These Reynolds numbers were chosen to be consistent with the other cases ran earlier. The heat fluxes on the other side were analyzed to compare the heat transfer rates at the same Reynolds number. It was evident that at lower temperatures, the heat transfer rates were greater than at higher temperatures.

Fig. 4-13 below shows the experimental contour for temperature along the stream wise direction of the test rig. As seen in the contour the temperature in the first half is much lower than the second half verifying that the temperature increases downstream of the channel.

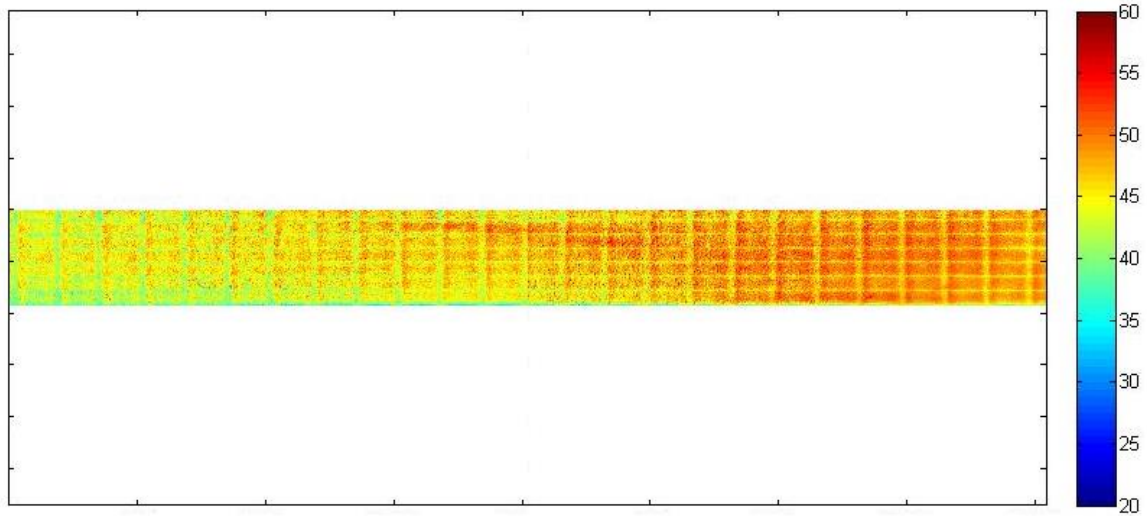


Figure 4-13: Experimental Contour for Temperature

As in case of the heat transfer, the trends just show the opposite. The Nusselt number starts to decrease down the channel. This happens due to the turbulent mixing of air upstream of the channel which tends to lose its cooling capability down the channel. Fig. 4-14 below shows the Nusselt number contours for the ribbed channel at a $Re=21,500$ and a heat flux of 1670 W/m^2 . Something to notice is the second heater strip from the top, which shows a little variation from the others, is because it might have an air bubble or a loose connection with the surface painted with TSP hence giving less intensity readings.

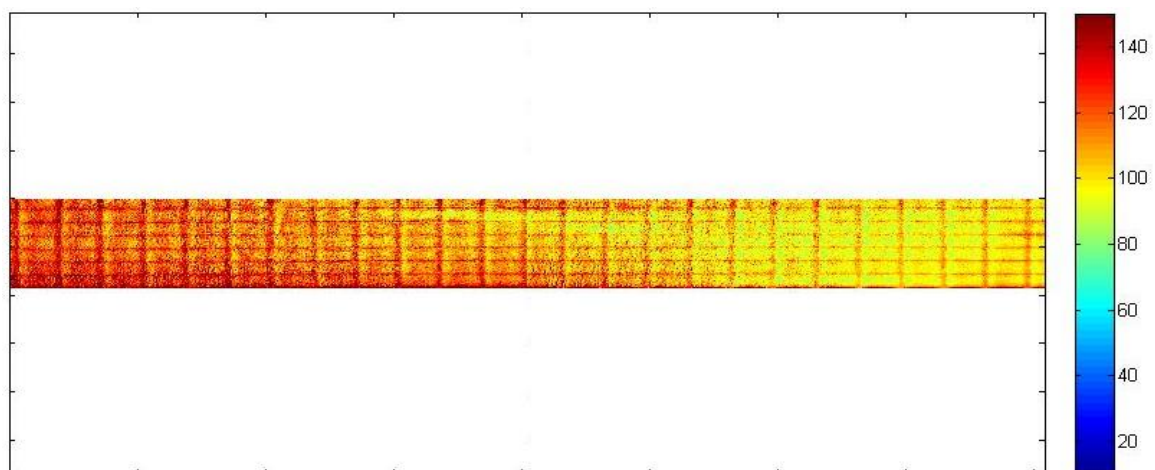


Figure 4-14: Experimental Contour for Nusselt Number

The heat transfer rates can be seen more clearly in the span averaged plots below.

Fig. 4-15, 4-16 compare the span averaged Nusselt number values plotted at a Re of 21,500 and 42,000. At a low Re, the CFD heat transfer rates very closely match with experimental values, validating the in house PTML rig. It is observed once again the sudden spikes in Nusselt numbers seen in CFD are not seen during experimental testing.

In case of the higher Re case, the Nusselt numbers plots do not line close to each other showing that at higher turbulence, the mixing of air is not as prominent as in case of the lower Re. This can be justified by looking at the peaks in between the 2 ribs. The value spikes very high making the reattachment length longer, hence have less interaction with the inner walls.

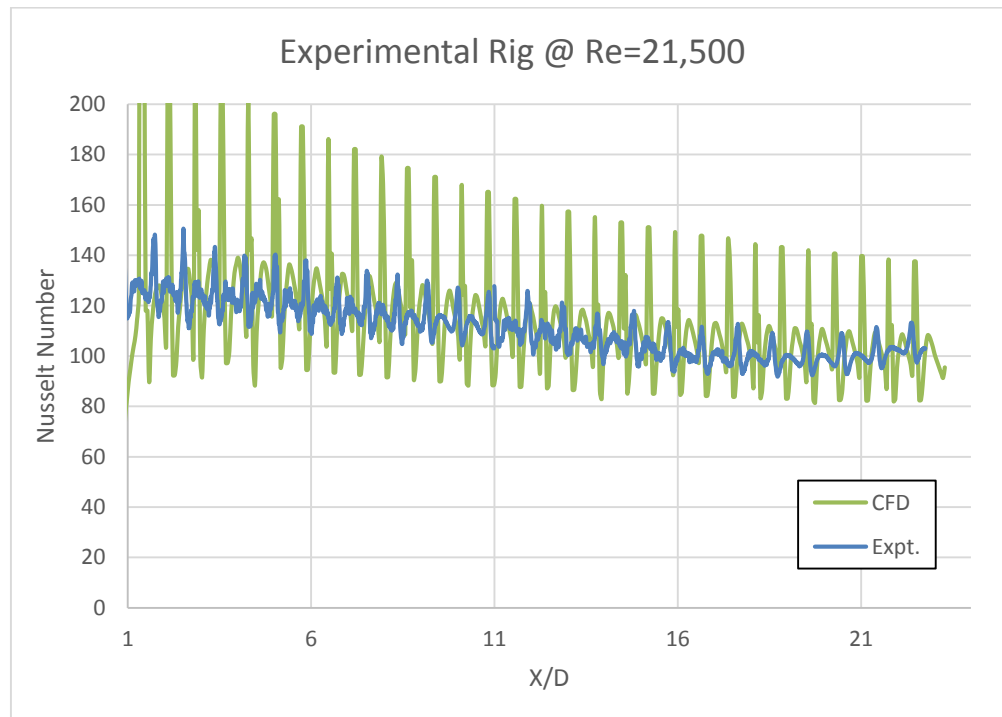


Figure 4-15: Experimental span averaged Nusselt Number along the bottom wall at Re = 21,500

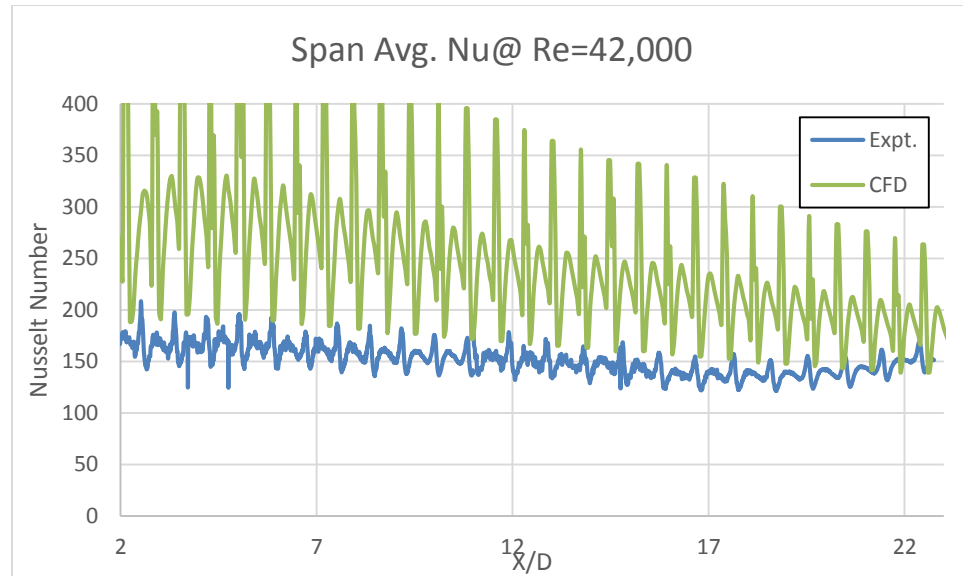


Figure 4-16: Experimental span averaged Nusselt Number along the bottom wall at $Re = 42,000$

It is noticed that the experimental results under predicts CFD. One of the reasons could be due to the use of a low conductive thermal tape which was used to stick a highly conductive aluminum rib. Also sudden spikes are seen at the leading edge of the rib in case of CFD is because lateral conduction wasn't accounted for.

5. Conclusion

The aim of this work was to benchmark the experimental results performed by J C Han to the computational fluid dynamics (CFD) results in a channel with rib turbulators and analyses the flow conditions. Followed by the preceding benchmarking, the best flow conditions are used to validate an in-house experimental rig for further optimization studies. Four commercially used turbulence models were compared, which showed that in case for a periodic ribbed channel with a $P/e = 10$ and an $e/D = 0.063$, the best results were seen in the V^2F turbulence model. This turbulence model match experimental results from Han's (1985) data within 5% of the experimental local Nusselt numbers and under predicted the friction factor by about 5.3%. In case of the difference of reattachment lengths, it was seen that even though EB $k-\epsilon$ wasn't close to the literature value, it showed higher heat transfer rates between the ribs. These cases were ran on the most mesh independent case with Y^+ less than one everywhere.

Friction factor comparison was done to validate the pressure profiles. In case of the EB $k-\epsilon$ turbulence model, both higher and lower Reynolds number values were within the uncertainty of Han's (1985) work. Further studies in is needed to compare more turbulence models with different Reynolds numbers and positioning of ribs in the channel before the best match can be determined.

The closest two turbulence models to match were V^2F and EB $k-\epsilon$. Due to the highly unstable nature of V^2F , it started deviating at higher Reynolds numbers. Hence the EB $k-\epsilon$ turbulence model was used to proceed with all the remaining cases. At a Re of 21,500, the experimental results very closely matched the CFD results validating the PTML rig testing facility. The purpose of validating the rig computationally helps in

reducing extensive experimentation of different configurations. With the help of CFD, various geometries, flow conditions and boundary conditions can be simulated in lesser time than needed.

Vast amount of research is done in the turbine engine and cooling technology. Increase in efficiency can be achieved by increasing the turbine inlet temperature. Keeping that goal in mind, this work was done in order to enhance the internal channels of a turbine blade using rib tabulators. By analyzing the data from this work it is evident that rib turbulated cooling enhances heat transfer with minimal pressure loss translating to greater operating turbine inlet temperatures.

6. Recommendations

Having validated the experimental rig to CFD, further studies in rib turbulated cooling will be an interesting topic to look into. Various geometries and configurations have already been looked into, so the next step into the rib roughened cooling would be rib optimization. In conjunction with the Undergraduate research team (IGNITE) a preliminary optimization study was carried out in STAR-CCM+ using a plugin called OPTIMATE+. This allows the user to optimize the rib in multiple disciplines. An assortment of geometries and rib configurations can be tested to investigate for higher heat transfer rates. Hence future work into rib optimization is something that should be looked into.

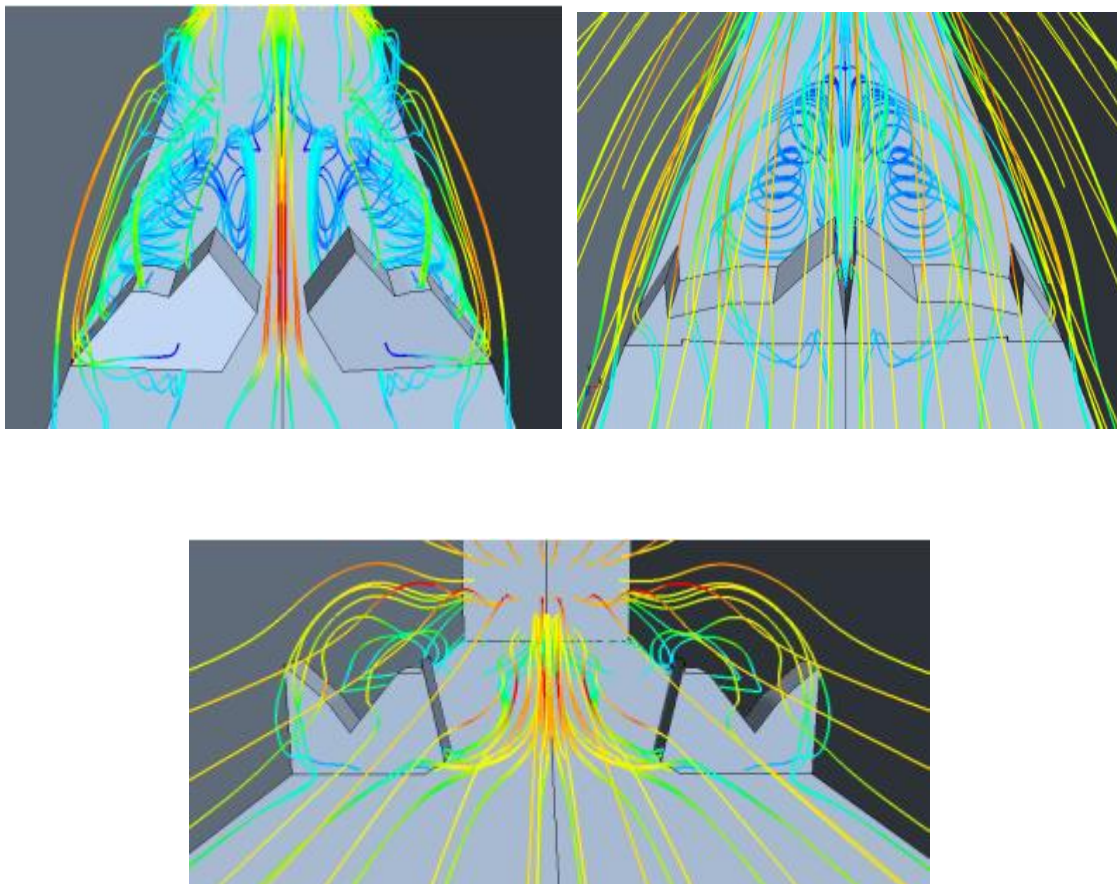


Figure 6-1: Images for different geometries tried in OPTIMATE+

7. Publications Resulting from this work

- Mehta, Yash, Ricklick, Mark, Ranade, I., Gutierrez, J. Guillen, E., 2015, “Development of Novel Internal Cooling Geometry for Gas Turbine Blades” Proceedings of the 2015 AIAA Science & Technology Forum and Exposition, Kissimmee FL. January 2015, AIAA 2015-0348
- Mehta, Yash, Ricklick, Mark, 2015, “CFD Benchmarking of Heat Transfer Predictions in Internal Channel with Rib Turbulators.” Proceedings of the 2015 AIAA Propulsion and Energy Conference 2015, Orlando FL. July 2015, AIAA 2015-3734

REFERENCES

- Bredberg, Jonas. "Turbulence Modelling for Internal Cooling of Gas-Turbine Blades." Web. 15 Sept. 2015.
- Buchlin, Jean-Marie. "Convective Heat Transfer in a Channel with Perforated Ribs." *International Journal of Thermal Sciences* 41.4 (2002): 332-40. Web.
- Chandra P. R.; Alexander C. R.; Han J. C.; 2003 "Heat Transfer and Friction Behaviors in Rectangular Channels with Varying Number of Ribbed Walls", *International Journal of Heat and Mass Transfer*, Vol. 46, pp. 481-495.
- Chklovski, Tara. "Pointed-Tip Wings at Low Reynolds Numbers." *Www.wfis.uni*. N.p., n.d. Web.
- Clifford, R.J., 1985. "Rotating Heat Transfer Investigations on a Multipass Cooling Geometry." AGARD CP 390.
- Davis, P. L., A. T. Rinehimer, and M. Uddin. "A Comparison of RANS-Based Turbulence Modeling for Flow over a Wall-Mounted Square Cylinder | CD-adapco." A Comparison of RANS-Based Turbulence Modeling for Flow over a Wall Mounted Square Cylinder | CD-adapco. *CD-Adapco*, 2012. Web. 08 June 2015.
- Dhanasekaran, T.s., and Ting Wang. "Computational Analysis of Mist/air Cooling in a Two-pass Rectangular Rotating Channel with 45-deg Angled Rib Turbulators." *International Journal of Heat and Mass Transfer* (2013): 554-64. Print.
- Dimensionless Wall Distance (y Plus). -- *CFD-Wiki, the Free CFD Reference*. Web. 2 Oct. 2015.
- Ekkad, S. V. and Han, J.-C., "Detailed Heat Transfer Distributions in Two-Pass Square Channels with Rib Turbulators," *International Journal of Heat and Mass Transfer*, Vol. 40, No. 11, 1997, pp. 2525–2537
- Florschuetz, L. W., Truman, C. R., Metzger, D. E., "Streamwise Flow and Heat Transfer Distributions for Jet Array Impingement with Cross flow," *Journal of Heat Transfer*, Vol. 103, 1981, pp. 337.
- Flynt, Guy A., Robert S. Webster, and Kidambi Sreenivas. "Computation of Heat Transfer in Turbine Rotor Blade Cooling Channels with Angled Rib Turbulators." *49th AIAA/ASME/SAE/ASEE Joint Propulsion Conference* (2013). Print.
- Han J. C.; Glicksman L. R.; Rohsenow W. M.; 1978 "An Investigation of Heat Transfer and Friction for Rib-Roughened Surfaces", *International Journal of Heat Mass Transfer*, Vol. 21, pp. 1143-1156.
- Han, J. C., J. S. Park, and C. K. Lei. "Heat Transfer Enhancement in Channels with

- Turbulence Promoters." *Journal of Engineering for Gas Turbines and Power* 107 (1985): 628. Print
- Han, J.C., 1988, "Heat Transfer and Friction Characteristics in Rectangular Channels with Rib Turbulators," *ASME Journal of Heat Transfer*, 110, pp. 321-328.
- Han, J.C. and Park, J.S., 1988, "Developing Heat Transfer in Rectangular Channels with Rib Turbulators" *International Journal of Heat and Mass Transfer*, 31 pp.183-195.
- Han J.C., S. Dutta, and S.V. Ekkad, "Gas Turbine Heat Transfer and Cooling Technology," Taylor & Francis, Inc., New York (2000)
- Han, J.C., and Chen, H.C., 2006, "Turbine Blade Internal Cooling Passages with Rib Turbulators," *J. of Propulsion and Power*, Vol. 22, No.2, pp. 226-248.
- Han, J.C., Zhang, Y.M., and Lee, C.P., 1991, "Augmented Heat Transfer in Square Channels with Parallel, Crossed, and V-Shaped Angled Ribs," *ASME Journal of Heat Transfer*, 113, pp. 590-596.
- Hyung Hee Cho, Kyung Min Kim, Jiwoon Song, "Applications of Impingement Jet Cooling Systems." Department of Mechanical Engineering, Yonsei University, Seoul, Korea, 2011.
- Kim, Hong-Min, and Kwang-Yong Kim. "Shape Optimization of Three-dimensional Channel Roughened by Angled Ribs with RANS Analysis of Turbulent Heat Transfer." *International Journal of Heat and Mass Transfer*: 4013-022. Print.
- Kim, Kwang-Yong, and Sun-Soo Kim. "Shape Optimization of Rib-roughened Surface to Enhance Turbulent Heat Transfer." *International Journal of Heat and Mass Transfer*: 2719-727. Print.
- Kim, Kyung Min, Yun Young Kim, Dong Ho Rhee, and Hyung Hee Cho. "An Investigation of Duct Aspect Ratio Effects on Heat/Mass Transfer in a Rotating Duct with 90° Ribs." *ASME Turbo Expo 2004 3 (2004)*: 483-92. Web.
- Kiml, Robert, Sadanari Mochizuki, and Akira Murata. "Effects of Rib Arrangements on Heat Transfer and Flow Behavior in a Rectangular Rib-Roughened Passage: Application to Cooling of Gas Turbine Blade Trailing Edge." *Journal of Heat Transfer* 123.4 (2001): 675-81. Web.
- Iacovides, H., and B.e. Launder. "Computational Fluid Dynamics Applied to Internal Gas-turbine Blade Cooling: A Review." *International Journal of Heat and Fluid Flow*: 454-70. Print.
- Park, J.S., Han, J.C., Huang, Y., Ou, S., and Boyle, R.J., 1992, "Heat Transfer Performance Comparisons of Five Different Rectangular Channels with Parallel

- Angled Ribs,” *International Journal of Heat and Mass Transfer*, 35, pp. 2891-2903.
- Rau, g.; Çakan, M.; Moeller, D.; Arts, T.; 1998 “The Effect Of Periodic Ribs on the Local Aerodynamic and Heat Transfer Performance of a Straight Cooling Channel”, *ASME Journal of Turbomachinery*, 120, pp 368-375.
- Ricklick, Mark A., and Cassandra Carpenter. "Comparison of Heat Transfer Prediction for Various Turbulence Models in a Pin Fin Channel." *50th AIAA/ASME/SAE/ASEE Joint Propulsion Conference* (2014). Print.
- Ricklick, Mark. "Characterization of an Inline Row Impingement Channel for Turbine Blade Cooling Applications." Web. 18 July 2015.
- Roberto Claret, Mark Ricklick and J. S. Kapat, “Computational and Experimental Comparison of Heat Transfer Characteristics of a Triple Row Impingement Channel at Large Impingement Heights”. Center for Advanced Turbines and Energy Research, 2011
- STAR-CCM+ Version 9.02.007 User Guide, CD-adapco Inc., New York, 2013.
- Sundberg, Jenny. "Heat Transfer Correlations for Gas Turbine Cooling." Web. 11 July 2015.
- Taslim, M. E., K. Bakhtari, and H. Liu. "Experimental and Numerical Investigation of Impingement on a Rib-Roughened Leading-Edge Wall." *J. Turbomach. Journal of Turbomachinery*: 682. Print.
- Taylor, J.R., “Heat Transfer Phenomena in Gas Turbines.” ASME Turbo Expo, GT-172, ASME, New Orleans, LA, 1980
- Wang L. B.; Tao W.; Wang Q.; Wong T. T.; 2001 “Experimental Study of Developing Turbulent Flow and Heat Transfer in Ribbed Convergent/Divergent Square Duct”, *International Journal of Heat and Flow*, Vol. 22, pp.603- 613.
- Wikipedia*. Wikimedia Foundation. Web. 30 Sept. 2015.
- Zhang, Q., P. M. Ligrani, and S. W. Lee. "Determination of Rough-surface Skin Friction Coefficients from Wake Profile Measurements." *Experiments in Fluids* (2003): 627-35. Print.
- Zuckerman N., Lior N., “Impingement Heat Transfer: Co-relations and Numerical Modeling”. *International Journal of Heat Transfer*, 2005

A. Appendix

Rig Drawings

